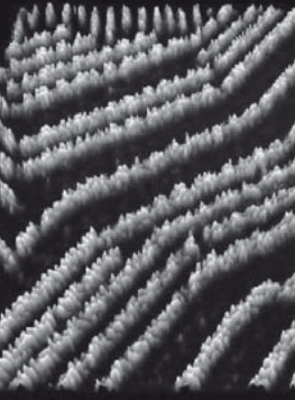

Chapter 3

Synthesis Routes

Learning objectives

- Different routes for the synthesis of nanoparticles and nanocrystalline materials
- Different routes for the consolidation of nanoparticles and nanocrystalline materials

There are different ways of classifying the synthesis routes for nanostructured materials. One of them is based on the starting state of material, namely, gas, liquid and solid. Techniques such as vapour condensation [physical vapour deposition (PVD) and chemical vapour deposition (CVD) and variants of these techniques] use the gaseous state of matter as the starting material for synthesizing nanoparticles. Techniques such as sol–gel, chemical and electrochemical (electrolytic) deposition and rapid solidification processing use liquids as the starting material. Severe plastic deformation processes such as high-energy ball milling, equichannel angular extrusion, etc., and nano-lithography, start with solids for synthesizing nanocrystalline materials.

However, the most popular way of classifying the synthesis routes is based on how the nanostructures are built, and such an approach leads to two routes, namely, the 'bottom-up' and the 'top-down' approaches. In the bottom-up approach, individual atoms and molecules are brought together or self-assembled to form nanostructured materials in at least one dimension. All the techniques that start with liquid and gas as the starting material fall into this category. In the second approach (top-down approach), a microcrystalline material is fragmented to yield a nanocrystalline material. All the solid state routes fall into this category.

Usually, the bottom-up techniques can give very fine nanostructures of individual nanoparticles, nanoshells, etc., with narrow size distributions, if the process parameters are effectively controlled. The top-down techniques do not usually lead to individual nanoparticles; however, they can produce bulk nanostructured materials. Many of the bottom-up approaches have difficulties in scale up, while the top-down approaches can be easily scaled up. Thus, one can see that both these approaches are complementary to each other, depending on the requirement of a particular application. The most prominent techniques to synthesize nanostructured materials are described.

B. S. Murty et al., *Textbook of Nanoscience and Nanotechnology,*
DOI 10.1007/978-3-642-28030-6_3, © Universities Press (India) Private Limited 2013

3.1 BOTTOM-UP APPROACHES

3.1.1 Physical vapour deposition (PVD)

PVD is a versatile synthesis method and is capable of preparing thin film materials with control at the nanometre scale by careful monitoring of the processing conditions. PVD involves the generation of vapour phase either via evaporation, sputtering, laser ablation or by using an ion beam. In *evaporation*, atoms are removed from the source, usually by heating it above its melting point. On the other hand, in *sputtering*, atoms are ejected from the target surface by the impact of energetic ions. Thermal evaporation has a limitation in multicomponent materials since one of the metallic elements typically evaporates before the other, due to the differences in boiling point and vapour pressure of the evaporating species. On the contrary, sputtering is capable of depositing high melting point materials such as refractory metals and ceramics, which are difficult to convert to nanomaterials by evaporation. Sputtering can result in better stoichiometric control of the film compared to evaporation techniques. Sputter-grown films usually have higher density than those obtained by evaporation as the sputtered atoms have more energy than the evaporated atoms. Sputtered films are more prone to contamination than evaporated films due to the lower purity of the sputtering target materials.

Inert gas condensation

(IGC) combined with thermal evaporation is commonly used to synthesise metallic and metal oxide nanopowders with a well-defined and narrow size distribution. This technique was originally introduced by Ganqvist and Buhrman in 1976 and later developed by Gleiter in 1981. In this process, a metal is evaporated inside an ultra-high vacuum (UHV) chamber filled with inert gas, typically helium (Fig. 3.1). The vapourised species then loses energy

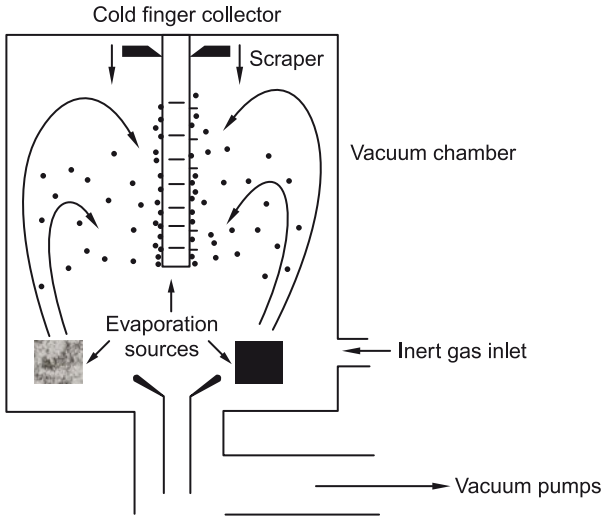

Fig. 3.1 Schematic inert gas condensation unit for the synthesis of nanocrystalline particles.

via collisions with helium molecules. As collisions limit the mean free path, supersaturation can be achieved above the vapour source. At high supersaturation, the vapours rapidly form large numbers of clusters that grow via coalescence and agglomeration. The clusters in the condensing gas are transported by convective flow to a vertical cold finger surface filled with liquid nitrogen. The removal of particles from the cold finger is carried out by a scraper assembly. They are collected via a funnel and transported to an in situ compaction device or coated with a surfactant agent that prevents them from agglomeration. The scraping and consolidation of particles are carried out under UHV conditions to prevent oxidation of the metallic nanoparticles. The size, morphology and yield of the clusters in gas condensation are dependent on three fundamental parameters:

- Rate of supply of atoms to the region of supersaturation where condensation occurs
- Rate of energy removal from the hot atoms via the condensing gas medium
- Rate of removal of clusters once nucleated from the supersaturated region

Particle nucleation, coalescence and growth during condensation also play key roles in forming small particles in large numbers.

As the yield of inert gas deposition is rather low, Bigot and co-workers developed a process wherein the metallic vapours condensed into a cryogenic medium to produce metallic nanocrystals. The main advantage of this technique is that it exhibits a higher production rate of about 60 g/h and a yield of 75%. Rapid overheating of the metal via radio frequency (RF) induction technique produces a high vapour pressure and substantial evaporation rate. The reactor is supplied continuously with cryogenic liquid, and nanoparticles are formed by rapid condensation of the supersaturated metal vapour. The condensation region, where the particles are formed by the nucleation, growth and coalescence processes, features a high temperature gradient—typically from 2200 K at the metallic surface to 77 K in the cryogenic medium. The low temperature of the surrounding medium produces a high rate of nucleation and rapid cooling of the as-formed particles limits crystal growth. Liquid argon is used for the synthesis of Al nanoparticles to prevent the formation of aluminium nitrides. Liquid nitrogen has been used for making Cu and Fe nanopowders. This technique yields Cu nanoparticles of spherical shape with their size distribution following a log-normal function peaking at 25 nm. The aluminium nanoparticles produced are also spherical, with size less than 70 nm.

IGC using a direct current (DC) or RF magnetron sputtering source has been used to prepare refractory metal and ceramic nanoparticles. The gas pressure, sputter power and source substrate distance are crucial process parameters during sputtering and gas condensation. A careful selection of these parameters will lead to the successful formation of nanoparticles rather than the formation of a granular film. The reported particle size is strongly dependent on argon pressure and for Mo, it decreases from 12 nm at 0.4 mbar to 5 nm at 0.8 mbar. Figure 3.2a shows nanocrystalline Ag–Cu deposit obtained by the IGC technique. The nanocrystalline nature of the Ag–Cu particles is clearly evident from the diffraction rings observed in the selected area electron diffraction pattern of Fig. 3.2b. Figures 3.2c–3.2f show the TEM micrographs of the deposit heated in situ to 200, 300, 400 and 600°C, respectively, in the TEM for understanding the grain growth behaviour of the

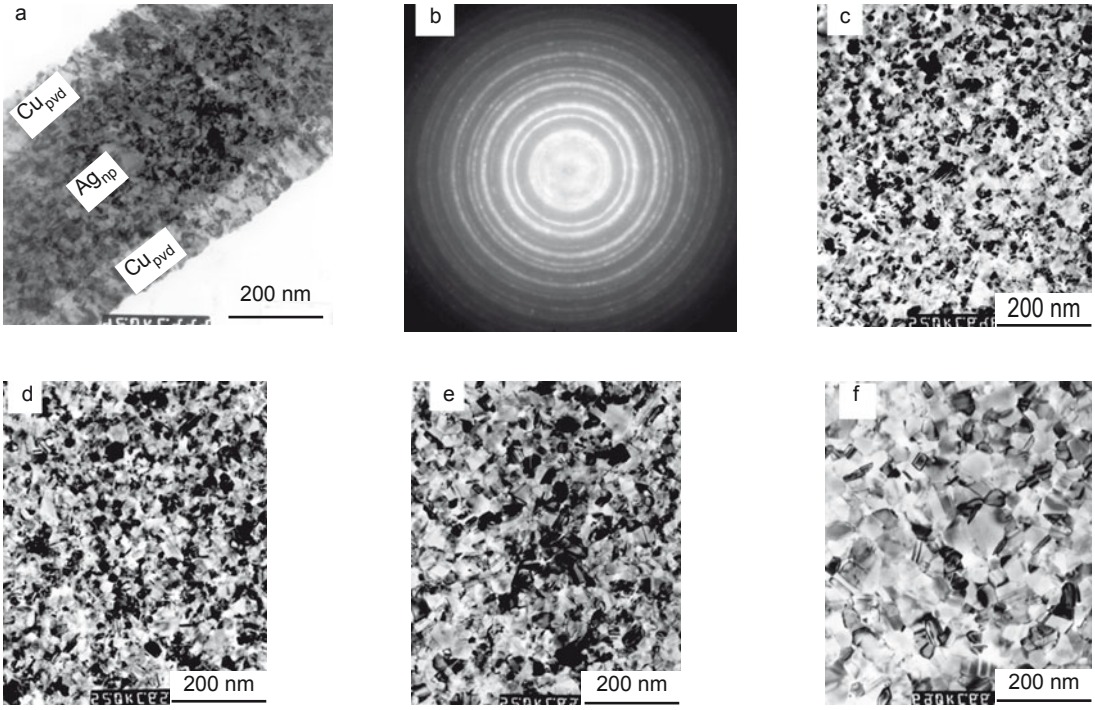

Fig. 3.2 Ag–Cu nanoparticles—(a) and (b)—synthesised by IGC and subjected to heating to (c) 200, (d) 300, (e) 400 and (f) 600°C. (*Source:* BS Murty, IIT Madras).

nanocrystalline deposit. The figure clearly indicates that nanocrystalline nature is retained in the deposit even after heating it to 600°C, due to the solute drag effect from the Cu present in Ag.

Laser ablation

It is generally known that laser ablation can provide better control of the evaporation process by congruent evaporation of constituent elements of multicomponent materials in a very short period of time. In this technique, an intense pulsed laser beam irradiates the target of interest, thereby vaporising atoms and clusters from the target. The total mass ablated from the target per laser pulse is usually referred to as the ablation rate. Laser ablation in combination with IGC is an attractive route to synthesize larger amounts of the multicomponent nanocrystalline materials. A typical laser ablation set up is shown in Fig. 3.3. In the process, atoms ablated by laser pulse tend to collide with helium gas, losing their kinetic energy rapidly. They eventually condense to form a cloud consisting of fine nanocrystalline clusters. The production rate of nanoparticles in this technique varies with helium gas pressure and laser pulse energy. Several workers have employed laser ablation and gas condensation to produce nanoparticles of metals, metal oxides and metal carbides.

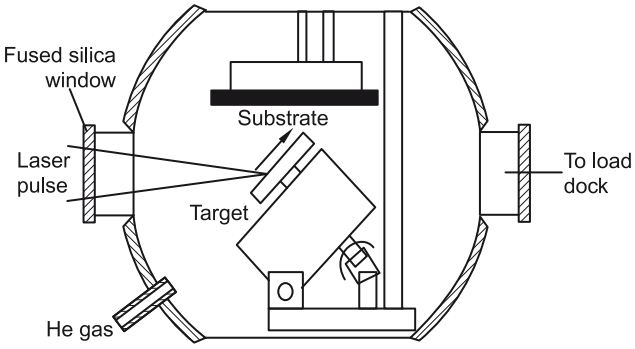

Fig. 3.3 Schematic of a laser ablation chamber equipped with a rotating target holder.

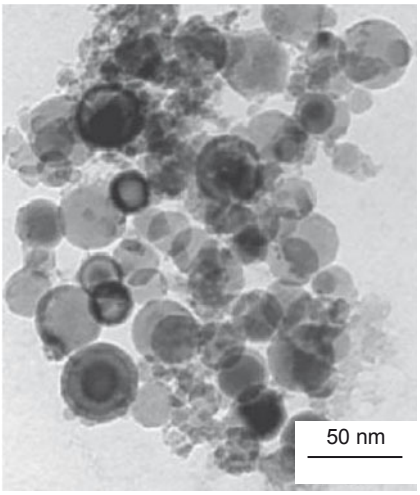

Fig. 3.4 Nanoparticles of Al synthesized by wire explosion technique.
(*Source:* R Sarathi, IIT Madras)

Wire explosion

Wire explosion technique is similar to physical vapour deposition. A fine wire of a metal is exploded by applying a very high voltage. The gas of atoms generated by this explosion is allowed to condense in the chamber to yield nanoparticles. This technique can lead to the formation of not only metallic nanoparticles but also a variety of oxides, nitrides, etc. by using different environments in the chamber. A typical example of nanoparticles generated by this technique is shown in Fig. 3.4.

3.1.2 Chemical vapour deposition

Chemical vapour deposition (CVD) is a process where one or more gaseous adsorption species react or decompose on a hot surface to form stable solid products. The main steps that occur in the CVD process can be summarized as follows:

1. Transport of reacting gaseous species to the surface
2. Adsorption of the species on the surface
3. Heterogeneous surface reaction catalysed by the surface
4. Surface diffusion of the species to growth sites
5. Nucleation and growth of the film
6. Desorption of gaseous reaction products and transportation of reaction products away from the surface

CVD is a more complicated method than PVD for the formation of thin films and coatings. It exhibits several distinct advantages, such as the capability to produce highly pure and dense films or fine particles at reasonably high deposition rates, and the capability of coating complex-shaped components uniformly due to its non–line-of-sight nature. A variety of

metallic, ceramic and semiconducting thin films are being deposited by CVD. Depending on the activation sources for the chemical reactions, the deposition process can be categorized into thermally activated, laser-assisted and plasma-assisted CVD.

Thermally activated CVD

This is the conventional CVD technique where the resistive heating of hot wall reactors gives sufficiently high temperatures for the dissociation of gaseous species. This leads to the heating of the entire substrate to a high temperature before the desired reaction is achieved. It precludes the use of substrates with melting points much lower than the reaction temperature. Hot tungsten filament is also used to heat the reacting gases in the vicinity of the substrate. Recently, hot filament CVD was used to grow one-dimensional SiC nanorods. Due to high hardness, high thermal stability, wide band gap and high electron mobility, SiC nanorods are potential materials for structural and electronic applications. Further, the Young's modulus of the nanorod can reach ~ 600 GPa, which is close to the theoretically predicted value for [111]-oriented SiC. In this CVD process, a silicon wafer was initially immersed in aqueous $Fe(NO_3)_3$ solution to remove the contaminants before transferring it into the reactor chamber. Carbon, silicon and silicon dioxide powders, compacted in the form of a plate, are used as the silicon and carbon sources. The chamber was filled with hydrogen gas and a tungsten filament was used to activate the hydrogen gas. The filament and substrate temperatures used are 2570 and 1373 K, respectively. The hot filament causes dissociation of molecular hydrogen to atomic hydrogen. The $Fe(NO_3)_3$ particles on the Si wafer surface were reduced by high concentration of atomic hydrogen to iron nanoparticles, which acted as a catalyst. In order to form hydrocarbon and silicon monoxide radicals, the silicon and carbon sources are thermally activated by hot filaments. The rods are straight with diameters of 20–70 nm and lengths of about 1 mm. Iron catalyst particles can be seen at the tips of the nanorods. HRTEM images revealed that the nanorods grew along the [100] direction. An electron bright field image of gold nanorods is shown in Fig. 3.5.

Plasma-enhanced CVD

This has a distinct advantage over thermal CVD due to its lower deposition temperature. The plasma is generated by various energy resources such as DC, RF, microwave and electron cyclotron resonance microwave (ECR-MW) radiation. In DC plasma, the reacting gases are ionised and dissociated by an electrical discharge, generating plasma consisting of electrons and ions. Microwave plasma is attractive because the excitation microwave frequency (2.45 GHz) can oscillate electrons. Thus, high ionization fractions are generated as electrons collide with gas atoms and molecules. SiC films have been deposited on silicon substrates by RF plasma-enhanced CVD using a gaseous mixture of $SiCl_4$, CH_4, H_2 and Ar. Recently, microwave plasma-enhanced CVD (MW-CVD) has been used to grow one-dimensional carbon nanotubes at a low temperature range of 600–800°C. Cold cathodes in field emission displays need well-aligned carbon nanotube arrays. The MW-CVD method has the advantage of achieving good alignment and selective growth on various substrates.

Conventional CVD of hydrocarbons over metal catalyst has been a typical method to produce various forms of carbon fibres, filaments and multiwalled nanotubes. In this process,

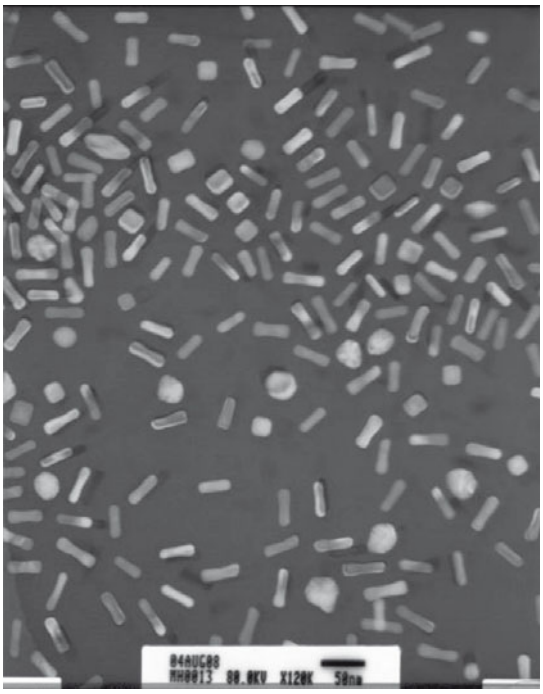

Fig. 3.5 Transmission electron micrograph of gold nanorods, along with a small fraction of impurities. (*Source:* http://commons.wikimedia.org/wiki/File:Au_nr_mhore.jpg.).

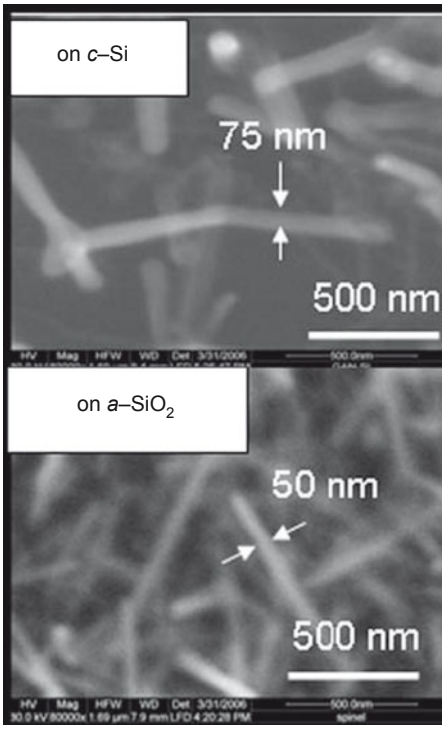

Fig. 3.6 GaN nanowires deposited by CVD on crystalline Si and amorphous silica. (*Source:* P Shankar, Saveetha University).

hydrocarbon molecules are absorbed and decomposed on transition metal (Fe, Ni, Co) particles. The carbon atoms diffuse into the interior of the catalyst to form a metal–carbon solid-state reaction. The precipitation of carbon from the supersaturated catalyst particle gives rise to carbon tube structure. Figure 3.6 shows GaN nanowires deposited by CVD on crystalline Si and amorphous silica.

Laser CVD is associated with the deposition of chemical vapours using a laser beam generated from sources like CO_2, Nd:YAG and Excimer. This process yields good quality films at lower temperatures with better control on composition. For example, a silicon nitride film could be deposited at 200°C using laser CVD, whereas it is deposited at 850°C and 450°C by thermally activated CVD and plasma-enhanced CVD, respectively. In the case of nanoparticles, tungsten powder of 54 nm could be synthesised from $WF_6/H_2/M$ (M = Ar, Kr, Ne, Xe) gas mixtures irradiated with an ArF Excimer laser. Moreover, ceramic Si–C–N nanometric powders can be obtained from laser-induced gas phase reactions of SiH_4, amines and NH_3. The incorporation of Si–C–N powders with sizes of 25–30 nm into aluminum improves its tensile and creep properties considerably. The box below describes a technique (molecular beam epitaxy) for precise formation of nanostructured thin films. There have also been attempts by people to

MOLECULAR BEAM EPITAXY (MBE)

MBE is a special case of evaporation for single crystal film growth, with highly controlled evaporation of a variety of sources in ultrahigh vacuum of about 10^{-10} torr. Besides the ultrahigh vacuum system, the MBE system usually consists of real-time structural and chemical characterisation capability, including reflection high energy electron diffraction (RHEED), x-ray photoelectric spectroscopy (XPS) and Auger electron spectroscopy (AES). Other analytic instruments may also be attached to the deposition chamber or to a separate analytic chamber, from which the grown films can be transferred to and from the growth chamber without exposure to the ambient atmosphere.

In MBE, the evaporated atoms or molecules from one or more sources do not interact with each other in the vapour phase under such low pressure. Although some gaseous sources are used in MBE, most molecular beams are generated by heating solid materials placed in source cells, which are referred to as *effusion cells* or *Knudsen cells*. The source materials are most commonly raised to the desired temperatures by resistive heating. The mean free path of atoms or molecules (100 m) far exceeds the distance between the source and the substrate (typically 30 cm) inside the deposition chamber. The atoms or molecules striking the single crystal substrate result in the formation of the desired epitaxial film. The extremely clean environment, the slow growth rate and independent control of the evaporation of individual sources enable the precise fabrication of nanostructures and nanomaterials as a single atomic layer. The ultrahigh vacuum environment ensures the absence of impurity or contamination, and thus a highly pure film can be readily obtained. Individually controlled evaporation of sources permits the precise control of chemical composition of the deposit at any given time. The slow growth rate ensures sufficient surface diffusion and relaxation so that the formation of any crystal defect is kept minimal.

ATOM MANIPULATION

In addition to imaging surface topography at atomic resolution, scanning tunnelling microscopy (STM) has the ability to carry out precise and controlled manipulation of atoms, molecules and nanostructures. The usual technique to manipulate atoms is to increase the current above a certain atom, which reduces the tip–atom distance, move the tip with the atom to a desired position, and finally to reduce the current again in order to decouple the atom and tip. The first demonstration of this technique was performed by Eigler and Schweizer (1990), who used Xe atoms on an Ni (110) surface to write the three letters 'IBM' on the atomic scale. Currently, many laboratories are able to move different kinds of atoms and molecules on different surfaces with high

precision. Controlled motion, pushing, pulling and sliding of the molecules depends on the tunnelling current, the distance and the particular combination of molecule and substrate. It is believed that the electric field between tip and molecule is the strongest force moving the molecules, but other mechanisms such as electromigration caused by the high current density or modifications of the surface potential due to the presence of the tip may also play an important role.

manipulate atoms and arrange them 'the way we want' as has been dreamt by Feynman. These efforts are described in the box above (atom manipulation).

3.1.3 Spray conversion processing

This route involves the atomization of chemical precursors into aerosol droplets that are dispersed throughout a gas medium. The aerosols are then transported into a heated reactor where the solution is evaporated to form ultrafine particles or thin films. This is an inexpensive technique as various low cost chemical solutions are available. Various aerosol generators—including pressure, electrostatic and ultrasonic atomisers—have been used for atomization purposes. These atomizers affect the droplet size, rate of atomization and droplet velocity. The most commonly used aerosol processing method is *spray pyrolysis*. In the process, aqueous solution is atomized in a series of reactors where the aerosol droplets undergo evaporation and solute condensation within the droplet; drying and thermolysis is followed by sintering. Nanoparticles can be prepared directly, synthesized from droplets or by liberating individual crystallites comprising the spray pyrolysis-derived particles from the thermolysis stage. Spray pyrolysis can be used to prepare several metal oxide nanoparticles such as ZnO, ZrO_2 and Al_2O_3.

Combustion flame spraying

Another type of gas condensation technique that uses liquid chemical precursors as the starting material is combustion flame spraying. The advantages of this process are low cost and high production rates. In the combustion flame spraying process, burning a fuel–oxygen mixture with a spray torch or flat-flame burner generates a flame. Chemical precursors are vapourised in the hot zone of the flame and pyrolysis occurs in the thin hot zone. The interaction between the flame and droplets yields nanoparticles. The use of a low-pressure chamber for the flat-flame burner precludes contamination and ensures the temperature profile across the entire burner surface is uniform. Low-pressure combustion flame spraying is often referred to as combustion flame chemical vapour condensation (CF-CVC). Solid, liquid and gaseous precursors can be used in this technique. CVC is an alternative to the inert gas phase condensation approach in which the evaporator in the IGC system is replaced by other sources such as burning flame, hot wall furnace and microwave plasma. The major advantage of plasma-assisted pyrolysis in contrast to thermal activation is the low reaction

temperature which reduces the tendency for agglomeration of nanoparticles. Combustion flame spraying has been used to produce a variety of high purity and non-agglomerated metal oxide nanoparticles such as TiO_2, Al_2O_3, ZrO_2, V_2O_5 and Y_2O_3–ZrO_2.

3.1.4 Sol–gel process

The sol–gel processing method has been in use for many years for producing metal oxide and ceramic powders with high purity and high homogeneity. The sol–gel route offers a degree of control of composition and structure at the molecular level. The process involves the generation of a colloidal suspension ('sol'), which is subsequently converted to viscous gel and solid material. Ebelman produced the first silica gel in 1846, and Cossa synthesized alumina gel in 1870. Since then, aerogels of zirconia, silazane, borate and other ceramics have been synthesized using the sol–gel technique.

In the process, reactive metal precursors were initially hydrolysed, followed by condensation and polymerization reactions. Metal alkoxides are metalorganic compounds with an organic ligand attached to a metal or metallic atom. They are the result of direct or indirect reactions between a metal M and an alcohol ROH. Typical examples are methoxide (OMe; $MOCH_3$) and ethoxide (OEt; MOC_2H_5). During hydrolysis, the alkoxy group OR is replaced by hydroxo ligands (OH), i.e.,

$$M(OR)_z + H_2O \longrightarrow M(OH)(OR)_{z-1} + ROH$$

where R is an alkyl group, C_nH_{2n+1}. The mechanism of this reaction involves the addition of a negatively charged $HO^{\delta-}$ group to the positively charged metal centre ($M^{\delta+}$) followed by the removal of ROH.

The factors that influence the hydrolysis reaction are:

- Nature of the alkyl group
- Nature of the solvent
- Concentration of each species in the solvent
- Temperature
- Water to alkoxide molar ratio
- Presence of acid or base catalysts

Subsequent condensation eliminates either water or alcohol to produce metal oxide or hydroxide linkages. In this process, two mononuclear complexes of M, each comprising only one metal M, can react with one another to form a polynuclear complex consisting of two metal atoms. Condensation occurs only when at least one hydroxo ligand is bonded to the cation M, and is designated as M-OH for simplicity. Olation and oxolation reactions lead to condensation. Olation is a reaction by which the hydroxo or 'ol' bridge (M–OH–M) is formed between two cations, while oxolation involves the formation of oxo bridges (M–O–M) between two metal cations:

$$\text{olation:} \qquad M - OH + M - OH_2 \longrightarrow M - OH - M + H_2O$$

$$\text{oxolation: } M - OH + H - OM \longrightarrow M - O - M + H_2O$$

$$M - OH + ROM \longrightarrow M - O - M + ROH$$

The 'ol' or 'oxo' bridges between two metal atoms lead to the formation of condensed oxide or hydroxide species. Under acid conditions, three-dimensional solid phase networks consisting of extended linear M–O–M chain polymers are developed. Inorganic polymerization is believed to occur in three stages during acid-catalysed condensation:

1. Polymerization of monomer units to form particles
2. Growth of particles
3. Linking of particles into chains, then solid networks that extend throughout the liquid medium, thickening it to a gel

In acid solution, the sol-to-gel transition allows the solid phase to be shaped into films, fibres and monoliths. For preparing coating films and fibres, the sol must exhibit spinnability. It appears that only solutions containing long-chained polymers are spinnable. Films are generally coated on the surface of the substrate via spin coating and dipping processes. Gel fibres are made by fibre drawing from the viscous alkoxide solution at or near room temperature. In contrast, on basic hydrolysis of metal alkoxides, a colloidal sol is generated. The gel is colloidal when the solid network is made of round sol particles.

Removal of the solvents and appropriate drying are important steps to achieve gel densification. When a solvent is evaporated from the gel under atmospheric conditions, capillary pressure due to the interfacial tension of the solvent places a high stress on the gel network. This leads to considerable shrinkage and fracture of the gel during drying. The resultant hard, glassy and porous product is called a *xerogel*. When the liquid within the gel is removed above its critical temperature and pressure (hypercritical) in an autoclave, the capillary pressure can be eliminated. The product thus obtained is referred to as an *aerogel*. An aerogel is generally amorphous and exhibits several unique properties such as high surface areas and porosities, and low densities and conductivities.

The most commonly studied metal alkoxide is silicon tetraethyl orthosilicate [TEOS; $Si(OC_2H_5)_4$]. The TEOS precursor can react readily with water via the following reaction:

$$Si(OR)_4 + H_2O \longrightarrow Si(OR)_3(OH) + ROH$$

As the hydrolysis of silicon alkoxides is very slow, the conversion of metal precursor molecules into trialkoxy silanol, $Si(OR)_3(OH)$ proceeds more rapidly by adding acid or base catalysts. Depending on the amount of water and catalyst present, hydrolysis may proceed partially, in which the metal alkoxides convert into $Si(OR)_{4n}(OH)_n$, or may go to completion in which all OR groups of alkoxides are replaced by OH:

$$Si(OR)_4 + 4H_2O \longrightarrow Si(OH)_4 + 4ROH$$

Subsequent condensation reaction sequences produce cluster species with Si–O–Si (siloxane) bonds and water or alcohol as the by-products:

$$(OR)_3Si - OH + HO - Si(OR)_3 \longrightarrow (OR)_3\, Si - O - Si(OR)_3 + H_2O$$

$$(OR)_3\, Si - OR + HO - Si\,(OR)_3 \longrightarrow (OR)_3\, Si - O - Si(OR)_3 + ROH$$

In silica aerogels, particles of 1–100 nm are arranged in a highly cross-linked silica solid network. In a recent study, colloidal silica particles were synthesized from hydrolysed TEOS, ethanol (C_2H_5OH) and de-ionised water using ammonium hydroxide (NH_4OH) as a catalyst. Silica nanoparticles can also be prepared simply via thermal decomposition, e.g., oxidation of TEOS or rice husk in a reactor, and the CF-CVC route as mentioned previously. Thermal decomposition of rice husk appears to be more cost effective due to global availability of cheap rice husk. Another process involves the precipitation of silica particles from the silicate solution and buffering with sulphuric acid.

Alkoxides of transition metals (e.g., titanium, zirconium) are highly reactive towards water. This implies that the rate of hydrolysis and condensation is very high, and thus it is difficult to form a stable sol of titania (TiO_2). Titania exists in three main crystallographic structures, namely, rutile, anatase and brookite. Among these, rutile is the only stable phase. Many acid catalysts such as nitric acid, hydrochloric acid and acetic acid have been added to lower the reaction rates. Apart from these acids, acetylacetone ($C_5H_8O_2$) can also moderate the reaction rate. It is added as a chelating agent to decrease the reactivity of titanium alkoxides and to form stable colloidal sols of ~ 5 nm. Under more controllable hydrolysis and condensation reactions, smaller particle sizes with more unique properties can be achieved. For example, TiO_2 aerogel nanocrystals can be obtained by supercritical evacuation of solvent from gels prepared through HCl-controlled hydrolysis condensation reactions of titanium isopropoxide in isopropanol. HCl catalyst favours the synthesis of titania powders with smaller grain size compared to acetylacetone catalyst under the same heat treatment conditions. Further, anatase crystallites are more stable if HCl is used as catalyst, while the pure rutile phase can be more easily obtained if acetylacetone is used as a catalyst. Figures 3.7a and 3.7b show the TEM micrographs of nanocrystalline titania prepared by the sol–gel route with a precursor to water ratio of 1 and 4, respectively. Figures 3.7c and 3.7d indicate that the nanocrystallite titania does not significantly grow on calcination up to about 500°C. According to the literature, various metal oxide nanocrystalline powders, e.g., SnO_2, $Ba_2Ti_2O_5$, $PbTiO_3$, (Pb, La)(Zr, Sn, Ti)O_3, nanocomposite powders containing elemental particulates, e.g., nano-Ni/SiO_2, Fe–Al_2O_3 and oxide nanocomposites, e.g., Fe_2O_3–SiO_2, NiO–SiO_2, and $3Al_2O_3$–$2SiO_2$, have been synthesized using the sol–gel process.

The sol–gel process has been useful for synthesizing only metal oxides as a result of the presence of metal–oxygen bonds in the alkoxide precursor, and the resulting gels are essentially metal hydroxides or oxides. This process has distinct advantages over other techniques for preparing metal oxide nanoparticles. These include the formation of high purity powders as a result of homogeneous mixing of the raw materials on the molecular level, and the large-scale industrial production of nanopowders. The disadvantage of the process is the high cost of alkoxide precursors. In some cases, the sol–gel route can also be used to prepare non-oxide ceramic powders such as β-SiC and ferroelectrics like (Pb, La)(Zr, Sn, Ti)O_3 (PLZST). In the

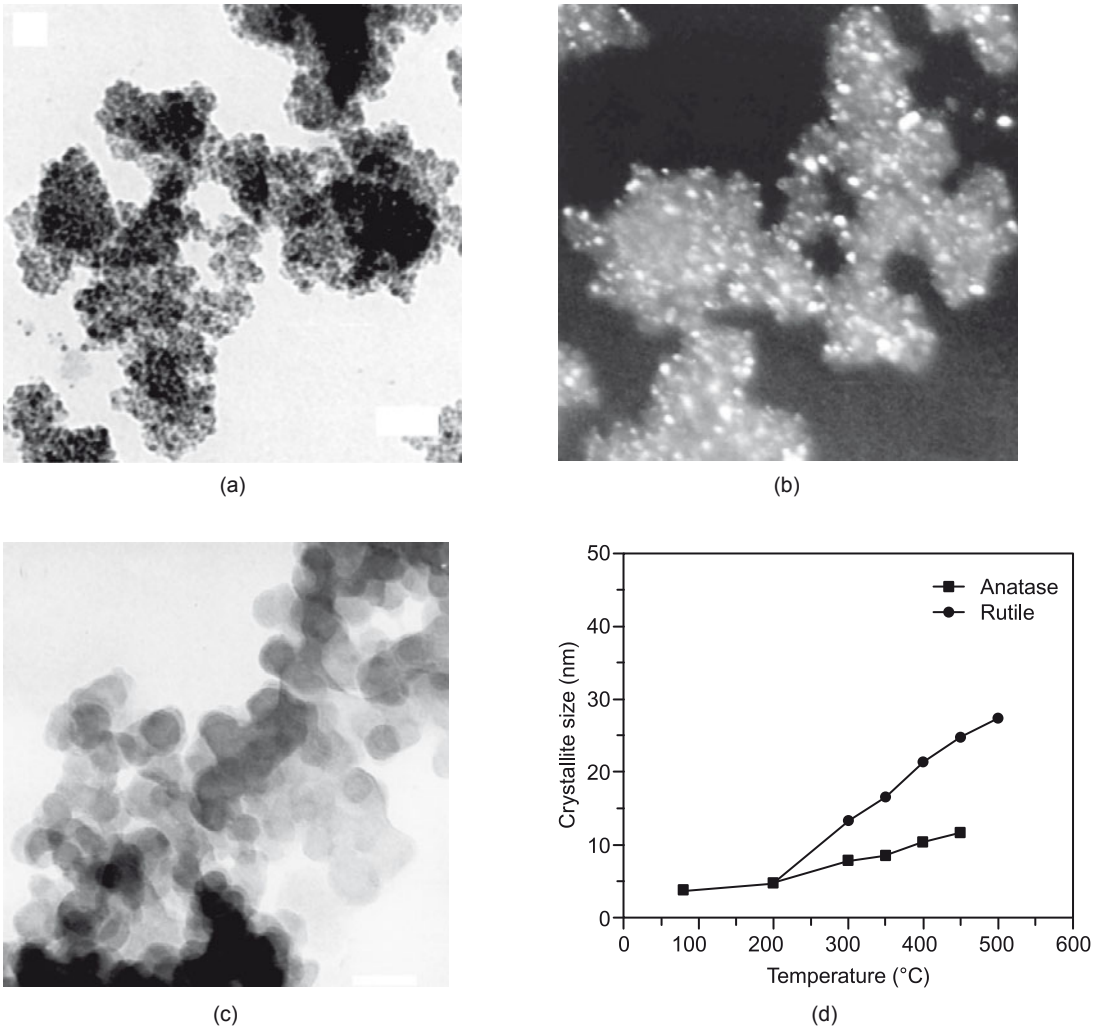

Fig. 3.7 TEM micrographs of nano titania (a) as-prepared (bright field image) with precursor to water ratio of 1, (b) as-prepared (dark field image) with precursor to water ratio of 4, (c) after calcination at 400°C for 2 h (bright field image) with precursor to water ratio of 4 and (d) Variation of the crystallite size of the anatase and rutile phases with calcination temperature with precursor to water ratio of 4. (*Source:* BS Murty, IIT Madras).

former case, heat treatment of the gel product at 1500°C in argon atmosphere resulted in 0.6 mm spherical agglomerates consisting primarily of particles of 40 nm in diameter. Recently, β-SiC nanopowders of 13–30 nm were synthesized by the chemical vapour reaction of the SiH_4–C_2H_4–H_2 system in the temperature range of 1423 K and 1673 K; the products were free from agglomeration. β-SiC powders can be made available at relatively low cost by the process of pyrolising rice husks at 1200–1500°C. The disadvantage is the larger size of β-SiC powders produced by this process, i.e., within micrometre range. It is worth noting that transition metal

nanorods can be made by reacting carbon nanotubes with volatile metal oxides or halides. Thus, β-SiC nanorods can be produced from reactions of carbon nanotubes with SiO or Si–I reactants. The preferred growth direction of these nanorods is [111], though rods with [100] growth are also observed at low reaction temperatures.

The anti-ferroelectric ceramics are promising candidates for new ceramic actuators because of their unique characteristics of big and isotropic strain changes under applied electric field, as well as shape memory effects. Nano-sized ceramics prepared by the sol–gel method are usually more homogeneous and reactive than those fabricated by conventional solid-state reactions since the mixing of the reagents occurs on a finer scale. The lower processing temperature is also helpful in minimising the PbO loss. One of the problems in lead-based complex perovskites is the evaporation of PbO at high temperatures, leading to undesirable phases. Sol–gel derived powders of single perovskite phase can be used to produce bulk ceramic samples after sintering at various temperatures.

3.1.5 Wet chemical synthesis

Solution-based processing routes used for the synthesis of nanoparticles include precipitation of solids from a supersaturated solution, homogeneous liquid phase chemical reduction and ultrasonic decomposition of chemical precursors. These processes are attractive due to their simplicity, versatility and availability of low cost precursors. Inorganic salt compounds used in the wet chemical synthesis routes are more versatile and economical than alkoxides employed in the sol–gel process. A typical example is the formation of nanocrystalline titania powders via hydrolysis of $TiCl_4$ at lower temperatures:

$$TiCl_4 + 2H_2O \longrightarrow TiO_2 + 4HCl$$

Once the solution becomes saturated, crystallization of titania takes place either through homogeneous or heterogeneous nucleation. In the latter case, crystal seeds are added to the solutions to promote the crystallization of titania nanoparticles.

Salt reduction is one of the most commonly adopted methods to generate the metal colloid particles. The process involves the dissolution of metal salts in aqueous or non-aqueous environments followed by the reduction of metal cations to the zero-valent state. The nature of the metal salts determines the kind of reducing agent to be applied. To produce transition metal nanoparticles, group 6 metal chlorides such as $CrCl_3$, $MoCl_3$ and WCl_4 are reduced with $NaBEt_3$ in toluene solution at room temperature to form metal colloids of high yield. A typical reaction for forming metal powders is given as:

$$MCl_x + xNaBEt_3 \longrightarrow M + xNaCl + xBEt_3 + \left(\frac{1}{2}x\right) H_2$$

where $x = 3$ for M = Cr and Mo; $x = 4$ for M = W. However, the reduction of the chromium, molybdenum and tungsten halides with either $LiBEt_3H$ or $NaBEt_3$ in tetrahydrofuran (THF) solution generates the corresponding metal carbides (M_2C) rather than the metals. In another

experiment, nanostructured $Fe_{50}Ni_{50}$ alloy has been synthesized by ultra-rapid autocatalytic chemical reduction of the corresponding transition metal ions in alkaline aqueous solution with hydrazine hydrate ($N_2H_4 \cdot H_2O$) at 353 K. The alloy powder is composed of spherical particles with 96 nm mean size diameter.

Metal nanoparticles can also be generated via ultrasonic and thermal decomposition of metal salts or chemical precursors. Recently, ultrasonic waves were employed to stimulate the chemical reactions of inorganic salts. Sonication of argon-saturated aqueous solutions of NaAuCl and $PdCl_2$ results in the formation of noble metal AuPd alloy nanoparticles. Power ultrasonic waves can stimulate certain novel chemical processes due to the formation of localised hot spots in the liquid of extremely high temperatures (~ 3000 K) and high pressures (~ 1000 atm). The main event in the process is the nucleation, growth and collapse of cavitation bubbles formed in the liquid. The cooling achieved during the cavitation collapse is estimated to be greater than 2×10^9 K. This process is commonly referred to as the sonochemical method. Transition metal nanoparticles can be produced via sonication of their respective chemical precursors. For example, $Ni(CO)_4$ has been sonicated under argon atmosphere to obtain amorphous nickel. Nanostructured α-Fe is usually synthesized either via sonication or thermal decomposition of $Fe(CO)_5$ solution. One disadvantage of the sonication process is the difficulty in controlling the resulting particle size and distribution due to the agglomeration of particles into a porous coral-like microstructure.

A number of traditional and herbal methods of materials processing could also possibly lead to nanostructure formation. The box overleaf gives the highlights of these routes.

3.1.6 Self-assembly

Self-assembly is a nanofabrication technique that involves aggregation of colloidal nanoparticles into the final desired structure. This aggregation can be either spontaneous (entropic) and due to the thermodynamic minima (energy minimization) energy minimization constraints, or chemical and due to the complementary binding of organic molecules and supramolecules (molecular self-assembly). Molecular self-assembly is one of the most important techniques used in biology for the development of complex functional structures. Since these techniques require that the target structures be thermodynamically stable, they tend to produce structures that are relatively defect-free and self-healing. Self-assembly is by no means limited to molecules or the nano-domain and can be carried out on just about any scale, making it a powerful bottom-up assembly and manufacturing method (multi-scale ordering). Another attractive feature of this technique relates to the possibility of combining the self-assembly properties of organic molecules with the electronic, magnetic and photonic properties of inorganic components.

The central theme behind the self-assembly process is spontaneous (physical) or chemical aggregation of colloidal nano-particles. Spontaneous self-assembly exploits the tendency of mono-dispersed nano- or submicro-colloidal spheres to organise into a face-centred cubic (FCC) lattice. The force driving this process is the desire of the system to achieve a

INDIAN TRADITIONAL METHODS OF NANOSTRUCTURE SYNTHESIS

Science and technology had significantly advanced in India in ancient times. Grant Duff, British Historian of India, observed "Many of the advances in the sciences that we consider today to have been made in Europe were in fact made in India centuries ago." One such Indian heritage in materials science is the rustless wonder, the Delhi Iron pillar, which has been standing for 1600 years without getting corroded. Another example of Indian excellence is Wootz steel, which is an extremely strong steel developed in India around 300 BC. This steel has been extensively used for making swords as it could cut a metal helmet into two pieces (popularly known as Damascus steel). Recently (*Nature*, 2006) Paufler's group from Technical University Dresden, Germany, reported the presence of carbon nanotubes and nanowires in Damascus steel. Similarly, it is also possible to produce carbon nanotubes and nanoparticles from

Carbon nanotubes and nanoparticles by the herbal route

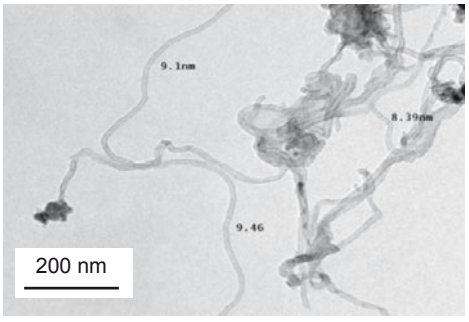

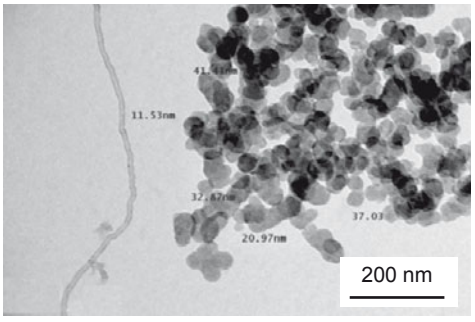

Copper nanoparticles by the herbal route

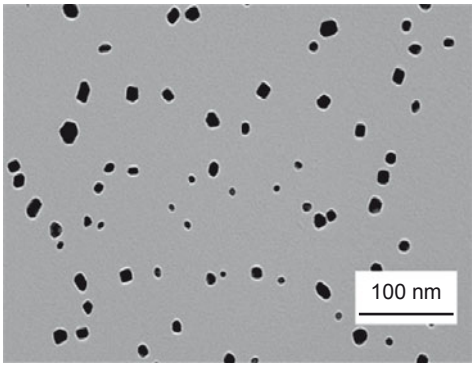

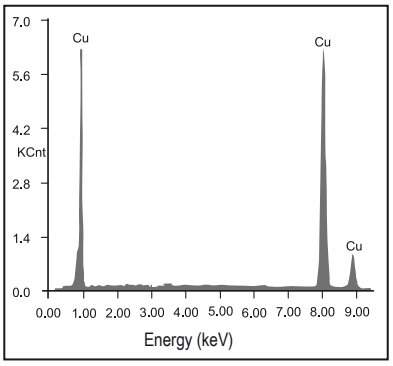

(*Source:* BS Murty, IIT Madras)

various vegetable oils, as shown in the images below. Such nanostructures appear to have been traditionally prepared in India.

Recently a Sanskrit scholar, Dr ABS Sastry, demonstrated the formation of copper nanoparticles by a simple chemical displacement reaction, where traditional herbs have been successfully used to cap the nanoparticles and prevent them from agglomeration. The transmission electron bright field image confirms the nanocrystalline nature of these copper particles. The energy dispersive x-ray spectrum from these individual nanoparticles confirms that they are pure copper.

thermodynamically stable state (minimum free energy). In addition to spontaneous thermal self-assembly, gravitational, convective and electro-hydrodynamic forces can also be used to induce aggregation into complex 3D structures. Chemical self-assembly requires the attachment of a single molecular organic layer (*self-assembled monolayer*, or *SAM*) to the colloidal particles (organic or inorganic) and subsequent self-assembly of these components into a complex structure using molecular recognition and binding.

Physical self-assembly

This method is driven by entropy that relies on the spontaneous organisation of colloidal particles into a relatively stable structure through non-covalent interactions. For example, Fig. 3.8 shows quinacridone molecules adsorbed on a graphite surface. The organic semiconductor molecules self-assemble into nanochains via hydrogen bonds. Natural assembly of on-chip silicon photonic band gap crystals, which are capable of reflecting the light arriving from any direction in a certain wavelength range, are also examples of this process. In this method, a thin layer of silica colloidal spheres is assembled on a silicon substrate. This is

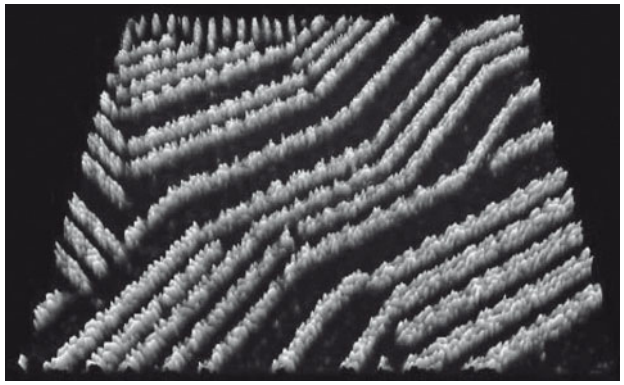

Fig. 3.8 Scanning tunnelling microscope image of quinacridone molecules adsorbed on a graphite surface. The organic semiconductor molecules self-assembled into nanochains via hydrogen bonds. (*Source:* http://commons.wikimedia.org/wiki/*File:*Selfassembly_Organic_Semiconductor_Trixler_LMU.jpg.).

achieved by placing a silicon wafer vertically in a vial containing an ethanolic suspension of silica spheres. A temperature gradient across the vial aids the flow of silica spheres. Once such a template is prepared, LPCVD can be used to fill the interstitial spaces with Si, so that the high refractive index of silicon provides the necessary band gap.

One can also deposit colloidal particles in a patterned substrate (template-assisted self-assembly, TASA). This method is based on the principle that when an aqueous dispersion of colloidal particles is allowed to de-wet from a solid surface that is already patterned, the colloidal particles are trapped by the recessed regions and assemble into aggregates of shapes and sizes determined by the geometric confinement provided by the template. The patterned arrays of templates can be fabricated using conventional contact mode photolithography, which gives control over the shape and dimensions of the templates, thereby allowing the assembly of complex structures from colloidal particles. This method can be used to fabricate a variety of polygonal and polyhedral aggregates that are difficult to generate.

Chemical self-assembly

Organic and supramolecular (SAM) molecules play a critical role in colloidal particle self-assembly. SAMs are robust organic molecules that are chemically adsorbed onto solid substrates. Most often, they have a hydrophilic (polar) head that can be bonded to various solid surfaces and a long, hydrophobic (non-polar) tail that extends outward. SAMs are formed by the immersion of a substrate in a dilute solution of the molecule in an organic solvent. The resulting film is a dense organization of molecules arranged to expose the end group. The durability of a SAM is highly dependent on the effectiveness of the anchoring to the surface of the substrate. SAMs have been widely studied, because the end group can be functionalised to form precisely arranged molecular arrays for various applications ranging from simple, ultra-thin insulators and lubricants to complex biological sensors. Chemical self-assembly uses organic or supramolecular SAMs as the binding and recognition sites for fabricating complex 3D structures from colloidal nanoparticles. Most commonly used organic monolayers include:

- Organosilicon compounds on glass and native surface oxide layer of silicon
- Alkanethiols, dialkyl disulfides and dialkyl sulfides on gold
- Fatty acids on alumina and other metal oxides
- DNA

Octadecyltrichlorosilane (OTS) is the most common organosilane used in the formation of SAMs, mainly because it is simple, readily available and forms good, dense layers. Alkyltrichlorosilane monolayers can be prepared on clean silicon wafers with a surface of SiO_2 (with almost 5×10^{14} SiOH groups/cm^2). Since the silicon chloride bond is susceptible to hydrolysis, a limited amount of water has to be present in the system in order to obtain good quality monolayers. Monolayers made of methyl- and vinyl-terminated alkylsilanes are autophobic to the hydrocarbon solution and hence emerge uniformly dry from the solution, whereas monolayers made of ester-terminated alkylsilanes emerge wet from the solution used in their formation. The disadvantage of this method is that if the alkyltrichlorosilane in the solvent adhering to the substrate is exposed to water, a cloudy film is deposited on the surface due to the formation of a gel of polymeric siloxane.

Another important organic SAM system is the alkanethiols $X(CH_2)_nSH$, where X is the end group) on gold. A major advantage of using gold as the substrate material is that it does not have a stable oxide, and can thus be handled in ambient conditions. When a fresh, clean, hydrophilic gold substrate is immersed (several minutes to several hours) in a dilute solution (10^{-3} M) of the organic sulphur compound (alkanethiols) in an inorganic solvent, a close-packed, oriented monolayer can be obtained. Sulphur is used as the head group, because of its strong interaction with gold substrate (44 kcal/mol), resulting in the formation of a close-packed, ordered monolayer. The end group of alkanethiol can be modified to render hydrophobic or hydrophilic properties to the adsorbed layer.

Another method for depositing alkanethiol SAM is soft lithography. This technique is based on inking a PDMS stamp with alkanethiol and its subsequent transfer to planar and non-planar substrates. Alkanethiol functionalised surfaces (planar, non-planar, spherical) can also be used to self-assemble a variety of intricate 3D structures.

Carboxylic acid derivatives self-assemble on surfaces (e.g., glass, Al_2O_3 and Ag_2O) through an acid–base reaction, giving rise to monolayers of fatty acids. The time required for the formation of a complete monolayer increases with decreased concentration. A higher concentration of carboxylic acid is required to form a monolayer on gold compared to Al_2O_3. This is due to differences in the affinity of the COOH groups (more affinity to Al_2O_3 and glass than gold) and also the surface concentration of the salt forming oxides in the two substrates. In the case of amorphous metal oxide surfaces, the chemisorption of alkanoic acids is not unique. For example, on Ag_2O the oxygen atoms bind to the substrate in a nearly symmetrical manner, resulting in ordered monolayers with a chain tilt angle from the surface normally of 15 to 25°. But on CuO and Al_2O_3, the oxygen atoms bind themselves symmetrically and the chain tilt angle is close to 0°. The structure of the monolayers is thus a balance of the various interactions taking place in the polymer chains.

Deoxyribonucleic acid (DNA), the framework on which all life is built, can be used to self-assemble nanomaterials into useful macroscopic aggregates that display a number of desired physical properties. DNA has a double-helix structure with two strands coiled around each other. When the two strands are uncoiled, singular strands of nucleotides are left. These nucleotides consist of a sugar (pentose ring), a phosphate (PO_4) and a nitrogenous base. The order and architecture of these components are essential for the proper structure of a nucleotide.

There are typically four nucleotides found in DNA: adenine (A), guanine (G), cytosine (C) and thymine (T). A key property of the DNA structure is that the described nucleotides bind specifically to another nucleotide when arranged in the two-strand double helix (A to T and C to G). This specific bonding capability can be used to assemble nanophase materials and nanostructures. For example, nucleotide functionalised nano-gold particles have been assembled into complex 3D structures by attaching DNA strands to the gold via an enabler or linker. In a separate work, DNA was used to assemble nanoparticles into macroscopic materials. This method uses alkane dithiol as the linker molecule to connect the DNA template to the nanoparticle. The thiol groups covalently attach themselves to the colloidal particles, leading to aggregate structures.

3.2 TOP-DOWN APPROACHES

3.2.1 Mechanical alloying

The mechanical alloying (MA)/milling process was originally developed by Benjamin of the International Nickel Company for the production of oxide dispersion strengthened (ODS) superalloys. It is now a widely used process for the fabrication of nanocrystalline powders. The possible spectrum of the uses of MA are shown schematically in Fig. 3.9. Recently, nanocrystalline high-entropy solid solutions with high hardness have been synthesized in multicomponent equiatomic alloys by MA.

Mechanical alloying or milling is usually carried out in high-energy mills such as vibratory mills (Spex 8000 mixer/mill), planetary mills (Fritsch and Retsch) and attritor mills (Szegvari attritor and Simoloyer). The vibratory mill has one vial, containing the sample and grinding balls and vibrates in all three directions. Because of the amplitude (about 50 mm) and speed (about 1200 rpm), the ball velocities are high (in the order of 5 m/s) and consequently the force of the ball's impact is unusually high. Another popular mill for conducting MA experiments is the planetary ball mill. In this mill, the vials rotate around their own axes and at the same time around the axis of a disc on which they are mounted. The centrifugal force produced by the vials rotating around their own axes and that produced by the rotating support disk together act on the vial contents, consisting of material to be ground and the grinding balls. Since the vials and the supporting disc rotate in opposite directions, the centrifugal forces alternately act in opposite directions. Due to this, the balls run down the inside wall of the vial. This is followed by the material being ground and grinding balls being lifted off and travelling freely through the inner chamber of the vial and colliding against the opposing inside wall. Grinding vials and balls are available in eight different materials—agate, silicon nitride, sintered corundum, zirconia, chrome steel, Cr–Ni steel, tungsten carbide and plastic polyamide.

An attritor ball mill consists of a stationary vertical drum in which a vertical shaft rotates with a series of horizontal impellers attached to it. Set progressively at right angles to each other, the impellers, through their rotation, energise the ball charge, causing powder size reduction

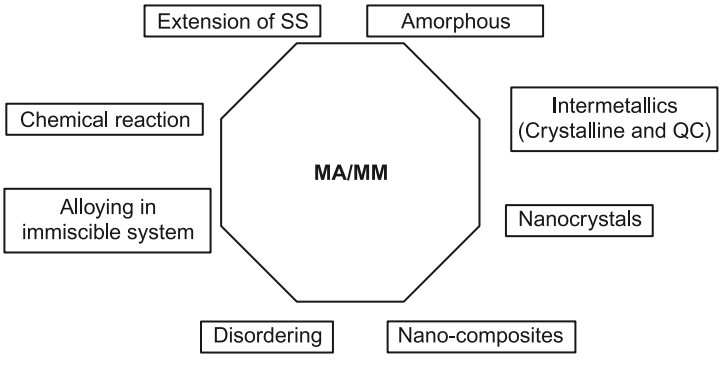

Fig. 3.9 Attributes of mechanical alloying or high-energy ball milling.

due to the impact between balls, between balls and the container wall, and between balls, the agitator shaft and impellers. Particle size reduction also occurs partially by interparticle collisions and by ball sliding on the walls of the vials. Attritors are the mills in which large quantities of powder (from about 0.5 to 40 kg) can be milled at a time. The most recent of the ball mills is the horizontal attritor (Simoloyer) that can be operated in dry processing at high relative velocity of the grinding media (up to 14 m/s) under controlled condition like vacuum or inert gas and in closed circuits. In these mills, the grinding media is accelerated by a horizontally arranged rotor inside the grinding vessel. These mills have the advantage of highest relative velocity of grinding media, which leads to high level of kinetic energy transfer, an intensive grinding effect and short processing times. The short processing times and collision-based grinding process results in low contamination levels. The simoloyers are available with 0.5- to 990-litre grinding chamber capacity, which makes it very convenient to scale-up the laboratory experiments to commercial production plants.

The mechanism of nanocrystallization during high-energy ball milling was first proposed by H.J. Fecht in 1983. He summarised the phenomenon of the development of nanocrystalline microstructure into three stages;

Stage 1: Localization of deformation into shear bands with high dislocation density.

Stage 2: Dislocation, annihilation and recombination to form nanometre-scale subgrains, which extend throughout the sample with further milling.

Stage 3: Transformation of subgrain boundary structure to randomly oriented high-angle grain boundaries. Superplastic deformation processes such as grain boundary sliding causes self-organisation into a random nanocrystalline state.

During high-energy milling, the powder particles are repeatedly flattened, cold welded, fractured and re-welded. Whenever balls collide, some amount of powder is trapped in between them. The impact from the balls causes plastic deformation of the powder particles, causing work hardening and fracture. The new surfaces formed by the fracture of the particles weld together. The composite particles at this stage have a characteristic layered structure consisting

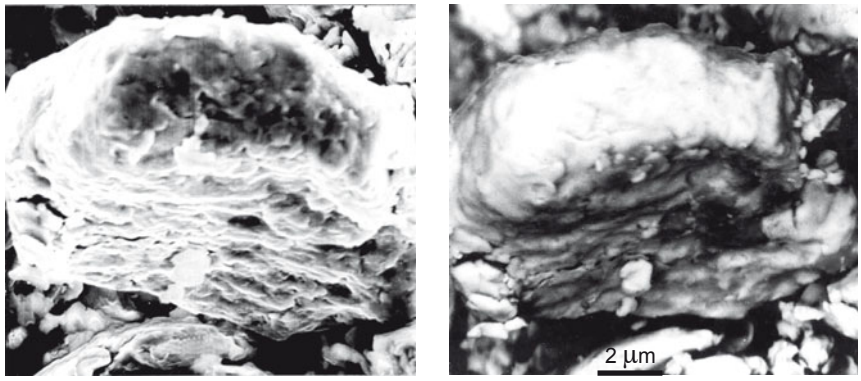

Fig. 3.10 (a) Secondary electron image and (b) backscattered electron image of layered structure observed during initial stages of high-energy ball milling of Ti and Al powder particles (*Source:* BS Murty, IIT Madras).

of various combinations of the starting constituents and are shown in Figs. 3.10a and 3.10b for the Ti–Al system. As deformation continues, the particles become work hardened and fracture. When fracture predominates over cold welding, the particle size is refined.

The minimum grain size achievable by high-energy ball milling has been related to several physical properties of elemental metals. It is reported that the minimum grain size, d_{min}, is inversely proportional to the melting temperature for low melting FCC metals. However, for HCP and BCC systems as well as FCC elements with melting temperature above that of Pd (1555°C), d_{min} appears to be insensitive to the melting point. For FCC metals, an inverse relationship was also found between d_{min} and bulk modulus, and a direct relationship between d_{min} and critical equilibrium distance between two edge dislocations. The majority of nanocryztalline metals have been synthesised to understand the mechanism of nanocrystallization and minimum grain size obtained by high-energy ball milling. Research has also been focussed on the validity of the Hall–Petch relation, and mechanical and physical properties of nanocrystalline metals. Fe, Cu, Ni, Pd, Cr, Nb, W, Hf, Ru, Zr, Co, Ag, Al, Si and graphite are among the few mentioned. Fecht et al, presented the first systematic report on the synthesis of nanocrystalline metals (Fe, Cr, Nb, W, Zr, Hf, Co and Ru) by high-energy ball milling. It is postulated that the grain boundary energy of the ball-milled nanocrystalline materials is higher than that of fully equilibrated grain boundaries.

An allotropic and polymorphic transformation induced by high-energy ball milling has been widely studied. High-energy ball milling of elemental Nb to a crystallite size of below 10 nm resulted in an allotropic transformation of BCC-Nb to FCC-Nb. Similar allotropic transformations such as HCP-Zr to FCC-Zr and HCP-Ti to FCC-Ti have been observed during high-energy ball milling by Manna and his group at IIT, Kharagpur. FCC to HCP transformation in Ni during high-energy ball milling was found to be aided by the addition of small amounts of Si and Al, which when dissolved in Ni can make it harder. A harder material can become nanocrystalline much more easily during high-energy ball milling due to extensive fracture when compared to a ductile material. Thus, the critical grain size of about 10 nm for the FCC to HCP transition in Ni could be achieved early during milling. It has been argued that the structural instability due to plastic strain, increasing lattice expansion and negative hydrostatic pressure was responsible for such transformations. Polymorphic transformations were also observed during high-energy ball milling of the $Ti_{50}Zr_{50}$ binary alloy. Transformation of quasicrystalline phase to crystalline BCC phase has also been observed in the Al–Cu–Fe and Al–Cu–Co systems. It was even observed in a number of systems such as Ti–Al, Ti–Ni, Ti–Cu, Fe—Si, etc., that nanocrystalline alloys below a certain critical size of about 10 nm (and above a critical lattice strain) can get structurally destabilised and become amorphous due to the large defect concentration.

Nanocrystallization by high-energy ball milling has also been demonstrated to help in extending the solid solubility of different solute elements into various solvent elements, as discussed in the previous chapter. This is basically due to the large fraction of grain boundaries in these nanocrystalline materials, which can accommodate large solute fractions.

Many ordered intermetallic compounds show high yield strength up to high temperatures and have the advantage of lower density compared to commercial superalloys. However,

these advantages are hampered due to their brittleness at low temperatures. It has been shown that the nanocrystalline intermetallics have improved formability. This finding has created an interest in the synthesis of several nanocrystalline aluminides, silicides and other intermetallics through MA. Interestingly, it has been observed that the phase fields of intermetallics can be significantly enhanced in the nanocrystalline state. In case of nanocrystalline NiAl synthesized by MA, the phase field NiAl has been extended from 45–55 at.%Ni in the conventional microcrystalline state to 25–65 at.%Ni in the nanocrystalline state. Similarly, studies on the Ni–Si, Fe–Si, Ni–Al, Al–Cu systems have indicated that only congruent melting compounds (which are expected to have lower surface energies) are expected to be stable in the nanocrystalline state.

It has also been observed that polymorphic transitions can be induced in intermetallics in the nanocrystalline state. Nayak and Murty synthesized the nanocrystalline $L1_2$–Al_3Ti intermetallic compound with the crystallite size less than 15 nm by MA of $Al_{67}M_8Ti_{25}$ (M = Cr, Mn, Fe, Co, Ni and Cu), while Al_3Ti usually has a DO_{23} structure. Among all the elements studied, Cu appears to be the best to stabilize $L1_2$–Al_3Ti. Another interesting observation was that the $L1_2$–Al_3Ti phase formed at an Al crystallite size of 15 nm. Similarly, $L1_2$–Al_3(Ti, Zr) compounds have formed at an Al crystallite size of about 20 nm, irrespective of the composition, as shown in Fig. 3.11. These observations clearly indicate that nanocrystallization is a prerequisite for the formation of intermetallic compounds. Figures 3.12a and 3.12b show the TEM dark field image and corresponding SAD pattern, respectively, obtained from nanocrystalline Al_3Zr.

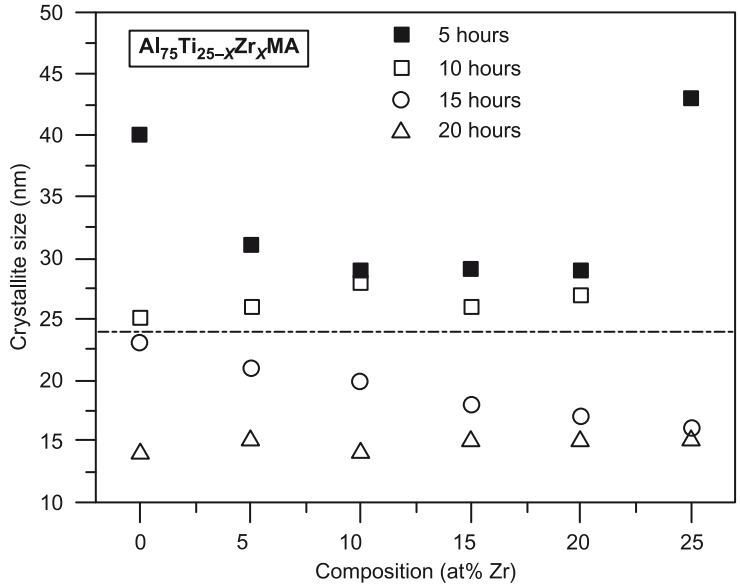

Fig. 3.11 Crystallite size of Al and intermetallic as a function of composition. Nanocrystalline intermetallic compound formation was observed when the crystallite size of Al was below 24 nm. The dotted line demarcates the phase field of mixture of elements and intermetallic compound. (*Source:* BS Murty, IIT Madras).

In situ nanocomposite formation by MA has found significant interest due to their potential application. It has been shown by Naser and his co-workers that no grain growth occurs in the matrix close to its melting point when Cu and Mg are reinforced with nanocrystalline Al_2O_3 by MA. In another interesting study, nanocomposites in the Al–Fe system have been synthesized by MA, which have shown exceptionally high hardness of about 13 GPa with densities very close to theoretical density. The very high hardness in these nanocomposites has been attributed to the presence of nanocrystalline/quasicrystalline intermetallic phases. Figure 3.13a shows the bright field image of nanocomposites in the Al–20Fe alloy. Detailed

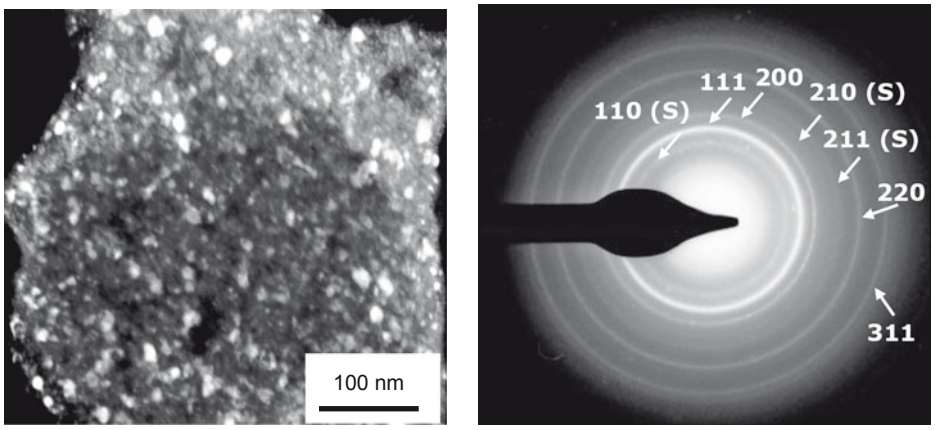

Fig. 3.12 TEM dark field image and corresponding diffraction pattern of $Li1_2$–Al_3Ti intermetallic. (*Source:* BS Murty, IIT Madras).

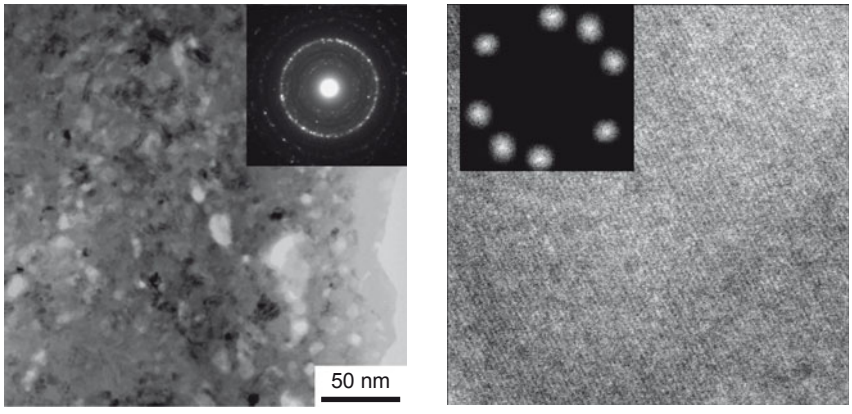

Fig. 3.13 (a) TEM bright field image of images of nanocomposites in Al–20Fe alloy after MA and subsequent annealing at 673 K for 2 h and (b) high resolution image, showing lattice fringes from nano-quasicrystalline particles in the Al matrix. (*Source:* BS Murty, IIT Madras).

high-resolution electron microscopy of these nanocrystalline intermetallics in this alloy indicated the possible presence of nano-quasicrystalline phase in these alloys, as shown in Fig. 3.13b.

Cu is a good electrical conductor; however, it has low strength due to which the life of Cu conductors as electrodes and as electrical contacts is quite short. Increasing the strength of Cu by using it in nanocrystalline form can improve the life of these conductors. However, nanocrystalline pure Cu can have significant grain growth at high temperatures. Cu-based nanocomposites such as Cu–W and Cu–Ta would be the answer to this problem. Figure 3.14a shows TEM evidence of the nanocrystalline nature of these Cu–20wt.%Ta nanocomposites. The AFM analysis of nanocomposites after sintering clearly showed that W and Ta can restrict the grain growth in Cu and retain the nanocrystalline grains. Figure 3.14b represents a typical AFM image of Cu–20wt.%W after sintering at 500°C. This indicates that even after sintering at about half the melting point of Cu, the nanocrystalline nature is retained in these nanocomposites. Interestingly, the nanocomposites could be sintered close to their theoretical densities at 500°C, while the micro-composies had to be sintered at temperatures close to the melting point of Cu for achieving similar densities as shown in Figs. 3.15a and 3.15b. These metal–metal nanocomposites synthesized by high-energy ball milling showed superior hardness and compressive strength without much reduction in conductivity. The Cu–W nanocomposites showed ~ 2.6 times higher hardness than microcomposites of similar composition. A similar observation is also made with Cu–Ta nanocomposites. Figure 3.16a shows the compressive strength of the Cu–Ta nanocomposites and microcomposites. The figure also shows the strength contribution (according to Hall–Petch equation) of the nanocrystalline grains. The Cu–Ta nanocomposites exhibited 3.6 to 5 times higher compressive strength than the microcrystalline composites of similar composition. The compressive strength of Cu–Ta nanocomposite is 4.5 to 7 times higher

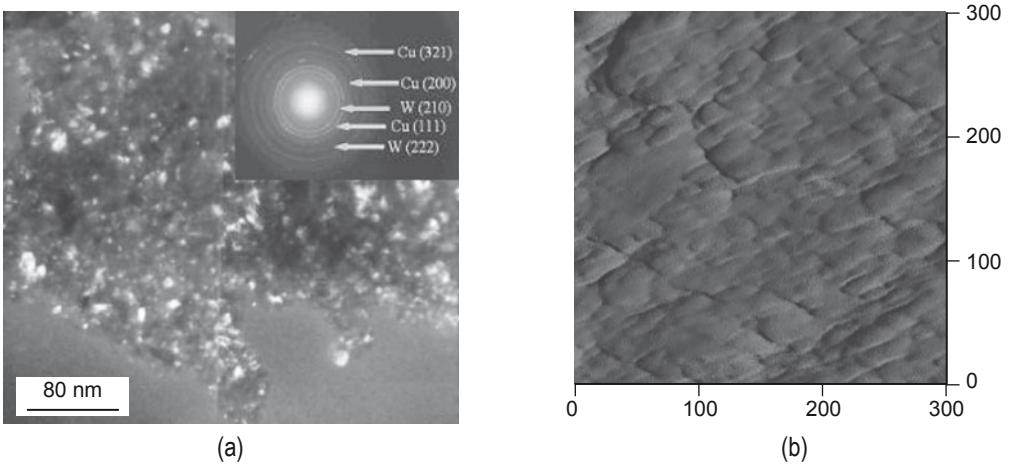

Fig. 3.14 (a) TEM image of Cu-20wt.%W ball-milled powders after 20 h of ball milling; (b) AFM analysis revealed nanograins in Cu-20wt.%W nanocomposites after sintering at 500°C for 2 h. (*Source:* BS Murty, IIT Madras).

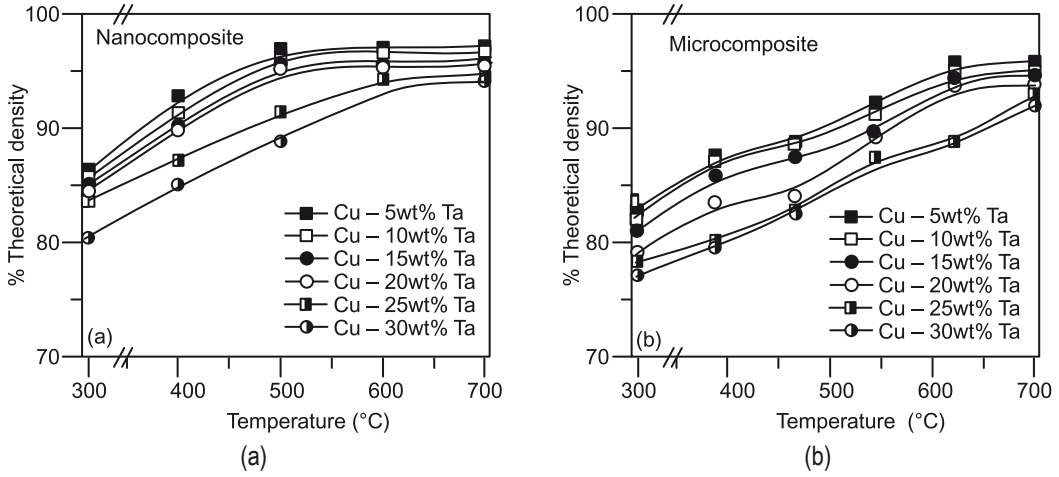

Fig. 3.15 Variation of density of Cu–Ta (a) nanocomposites and (b) microcomposites as a function of sintering temperature. (*Source:* BS Murty, IIT Madras).

than that of microcrystalline Cu, as shown in Table 3.3. The resistivity values of Cu–Ta nanocomposites (Fig. 3.16b) indicate that the major contribution of resistivity is due to Ta rather than fine grain size. Figure 3.17 shows the hardness to resistivity ratio of Cu–Ta nanocomposites normalized with that of the oxygen-free high conductivity (OFHC) Cu, which clearly indicates that the hardness on nanocomposites is three times higher than that of OFHC Cu for similar resistivity.

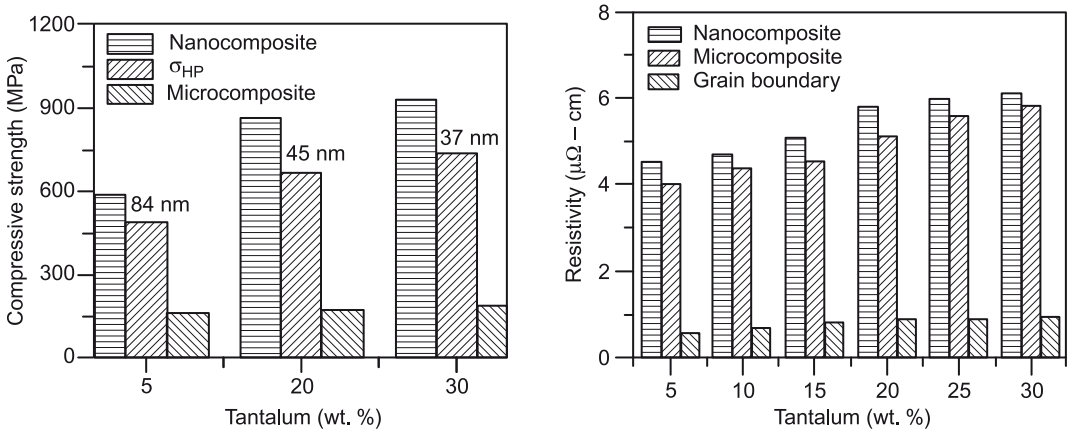

Fig. 3.16 (a) Compressive strength and (b) electrical resistivity of Cu–Ta nanocomposites synthesized by high-energy ball milling. (*Source:* BS Murty, IIT Madras).

Table 3.3 Compressive strength of Cu matrix nanocomposites

Vol. % / wt. % of dispersoids	Nanocomposite (MPa)	Microcomposite (MPa)	Increase wrt microcomposite	Increase wrt microcrystalline Cu (130 MPa)
Cu–Al_2O_3				
5.0/2.3	501	182	2.8	3.9
10.0/4.7	633	221	2.9	4.9
20.0/10.0	853	275	3.1	6.6
Cu–W				
2.4/5.0	536	168	3.2	4.1
11.6/20.0	770	229	3.4	5.9
16.5/30.0	853	284	3.0	6.6
Cu–Ta				
2.7/5.0	586	164	3.6	4.5
11.8/20.0	870	174	5.0	6.7
18.7/30.0	930	185	5.0	7.1

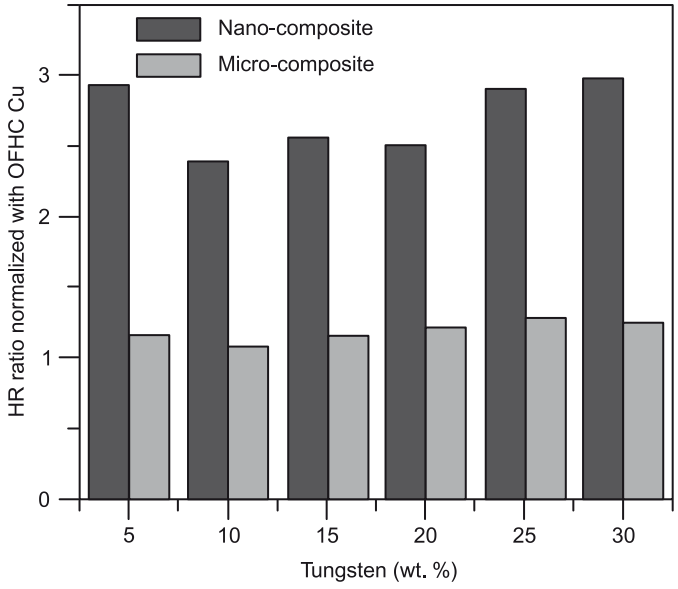

Fig. 3.17 Hardness to resistivity ratio of Cu–Ta nanocomposites normalized with oxygen-free high conductivity (OFHC) Cu. (*Source:* BS Murty, IIT Madras).

3.2.2 Equal channel angular pressing (ECAP)

The principle of ECAP [or equal channel angular extrusion (ECAE)] is illustrated schematically in Fig. 3.18. For the die shown in the illustration, the internal channel is bent through an

abrupt angle, ϕ, equal to 90°, and there is an additional angle, ψ, equal to 0° in Fig. 3.19, which represents the outer arc of curvature where the two channels intersect. In this process, a rod-like sample is pressed through the die using a plunger. Shear deformation occurs as the sample passes through the die. Despite the introduction of an intense strain as the sample passes through the shear plane, the sample ultimately emerges from the die without experiencing any change in the cross-sectional dimensions.

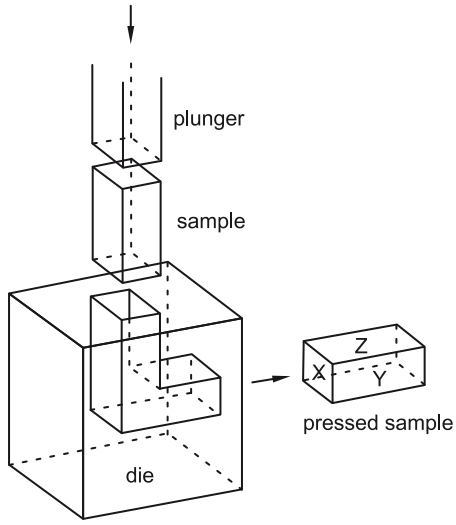

Fig. 3.18 Schematic illustration of ECAP facility.

Researchers all over the world are now studying the ECAE process as it is easy to install and does not require special equipment in the laboratories, except for the dies and a press machine. The ECAE process has been applied to various kinds of metals and alloys and has succeeded in producing ultrafine grain (UFG) microstructures (Fig. 3.19). However, the major materials used are light metals like Al- and Mg-alloys and the trials for steels are limited. This is presumably because large force is required to put the materials through the channel die, overcoming large flow stress and frictional stress. The hydrostatic compressive stress field in the ECAE process is an advantageous point to prevent fracture of the materials. However, cracking due to shear localization has been reported in less workable materials such as Ti–Al–V alloy.

Though the ECAE can fabricate bulk materials, the typical size of the samples is small. Further, the ECAE is principally not a continuous process but a batch process. A few experiments to make the ECAE continuous have been attempted (Fig. 3.20). Saito and

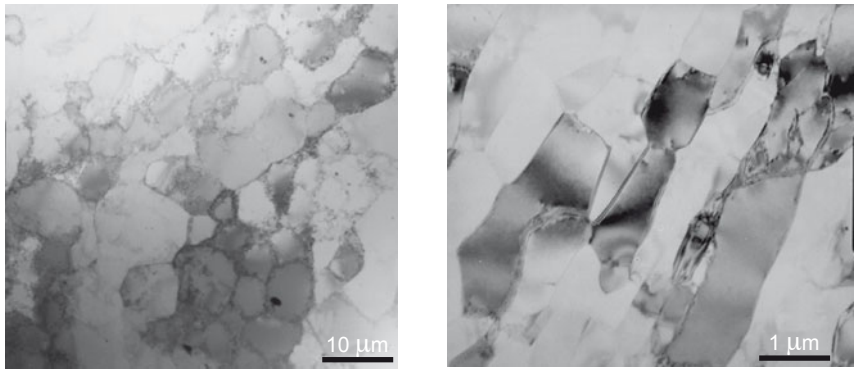

(a) (b)

Fig. 3.19 Microstructure of (a) annealed CP aluminum and (b) after ECAP. (*Source:* Uday Chekkingal, IIT Madras).

his co-workers developed the *conshearing process* for continuous ECAE of sheet metals (Fig. 3.20a). They equipped the ECAE die at the end of the satellite mill they previously invented. The *satellite mill* is the special rolling mill which can maintain the rotating speed of all the satellite rolls constant. As a result, compression force along the rolling direction (RD) appears in the materials between adjacent satellite rolls. Folding of the materials is prevented by the guide shoe equipped between the satellite rolls. The compression force in the satellite mill was used to put the sheet into the ECAE die. The conshearing was applied to obtain aluminium of commercial purity up to four cycles and succeeded in fabricating sound sheets, but UFG microstructures have not been obtained. Because they used sheet material, it was probably not effective to impose ideal shear strain owing to the bending and bending-back deformation and friction. Further, it is difficult to make the channel angle 90° in this configuration (they used 125°). On the other hand, the processed materials showed unique textures.

Lee and co-workers developed another continuous ECAE process, named the dissimilar channel angular pressing (DCAP) process, which is principally the same as conshearing (Fig. 3.20b). They used a conventional two-high mill, but the surface of the lower roll was mechanically roughened in order to feed the material into the ECAE die. As a result, the surface quality of the specimens would be worse than the conventionally rolled materials. Strips of 1.55 × 20 × 1000 mm were processed by the continuous confined strip shearing process and the UFGs similar to those obtained in the conventional ECAE have been reported in 1050-Al, though the difficulties and the disadvantages are not obvious from the limited publications currently available. The channel angle was varied from 100° to 140°, and it was found that the critical strain to form the UFGs increases by increasing the angle.

3.2.3 High-pressure torsion (HPT)

A method for fabrication of disc-type bulk nanostructured samples using high-pressure torsion is shown in Fig. 3.21. In HPT, the sample disk is strained in torsion under the applied pressure (P) of several GPa between two anvils. A lower holder rotates and surface friction forces the ingot to deform by shear. Due to the specific geometric shape of the sample, the main volume of the material is strained in conditions of quasihydrostatic compression under the applied

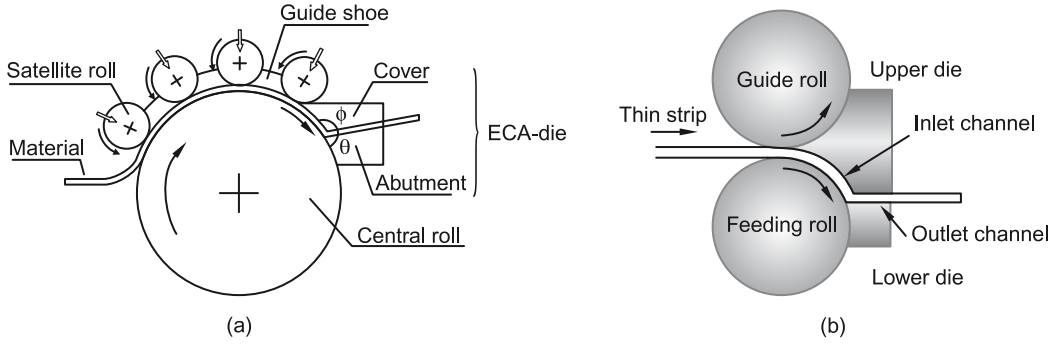

Fig. 3.20 Principle of (a) conshearing and (b) dissimilar channel angular pressing process.

pressure and the pressure of sample outer layers. As a result, in spite of large strain values, the deformed sample is not destroyed. Various strains can be achieved by rotating the lower anvil through a defined angle. The shear strain γ may be simply estimated as,

$$\gamma = \frac{2\pi RN}{d}$$

where R is the distance from the sample centre, N is the number of anvil rotations and d is the thickness of the sample. In this method of microstructure refinement, the simple shear stress conditions are realised at relatively low temperatures under high applied pressure (5–15 GPa). The samples fabricated by severe torsion straining are usually disc-shaped, with a diameter of 10 to 20 mm and thickness 0.2±0.5 mm. A significant change in the microstructure is observed already after deformation by 1/2 rotation, but for formation of the homogeneous nanostructure, as a rule, several rotations are required.

Using high-pressure torsion, the first nanocrystalline structures were developed in single crystals of Ni and Cu. It was found that the mean grain size had gradually decreased with increasing shear strain and had finally stabilized at the level of ~ 100 nm. Further experiments with initially coarse grained Cu, Ni, Fe, Cr and Ti revealed that strong grain refinement can be achieved in all these metals after 3–5 revolutions, whereupon the mean grain size usually reaches the steady state value of 100–200 nm, depending on the material (Table 3.4). Slightly smaller grain size has been reported for single phase matrix Fe and Al alloys and significantly smaller grain size, down to 10 nm, can be obtained for some multiphase alloys and intermetallic compounds.

Recent investigations also showed that severe torsion straining can be used successfully not only for the refinement of a microstructure but also for the consolidation of powders. It was revealed that during torsion straining at room temperature, high pressures equal to several GPa can provide a rather high density close to 100% in the processed disc-type nanostructured samples. For fabrication of such samples via severe torsion straining

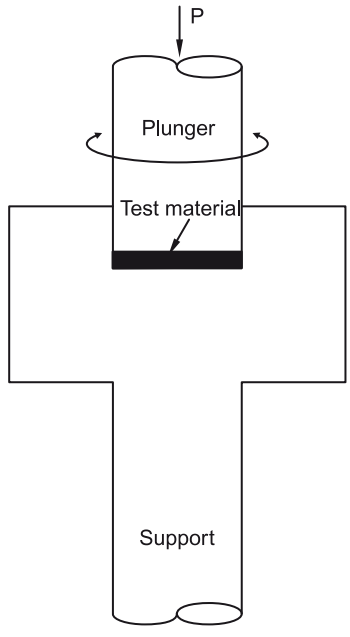

Fig. 3.21 Principle of high pressure torsion.

Table 3.4 Grain size of various kinds of HPT processed metals

Metal	Details of HPT processing	Grain size (nm)
Ni	P = 6 GPA, γ = 300, *RT*	170
Cu	P = 5 GPA, γ = 300, *RT*	200
Cu	P = 8 GPA, γ = 250, *RT*	200
Fe	P = 5 GPA, γ = 600, *RT*	100
Fe	P = 5 GPA, γ = 420, *RT*	127
Cr	P = 7.8 GPA, γ = 120, T = 623 K	500
Mo	P = 6 GPA, γ = 300, T = 623 K	190
Ti	P = 5 GPA, γ = 600, *RT*	120

consolidation, not only conventional powders but also powders subjected to ball milling can be used. The HPT consolidation of nanostructured Ni powder prepared by ball milling can be given as an example. The conducted investigations showed that the density of the fabricated powders is close to 95% of the theoretical density of the bulk coarse-grained Ni. TEM examinations showed the absence of porosity with a mean grain size of about 20 nm. It is also very interesting that the value of microhardness of the Ni samples fabricated by HPT consolidation is as high as 8.6 GPa.

3.2.4 Accumulative roll bonding (ARB)

Accumulative roll bonding is the only SPD process using rolling deformation itself (Fig. 3.22). Rolling is the most advantageous metal working process for continuous production of plates, sheets and bars. However, the total reduction applied to the materials is substantially limited because of the decrease in the cross-sectional dimension of the materials with increasing reduction. In the ARB process, a 50% rolled sheet is cut into two, stacked to the initial thickness, and then rolled again. As is evident, the rolling in the ARB is not only a deformation process but also a bonding process (roll bonding). To achieve good bonding, the surface of the materials is degreased and wire brushed before stacking, and the roll bonding is sometimes carried out at elevated temperatures below the recrystallization temperature of the materials. Repeating this ARB process a number of times can lead to very large plastic strain in the materials.

It has been observed that achieving good bonding is the critical step in the ARB process. Surface treatment is indispensable for achieving good bonding. Furthermore, there is a critical rolling reduction in one-pass roll bonding, below which it is difficult to achieve sufficient bonding. Though the critical reduction depends on the materials and the processing temperatures, more than 35% reduction by one pass is necessary in general, so that the

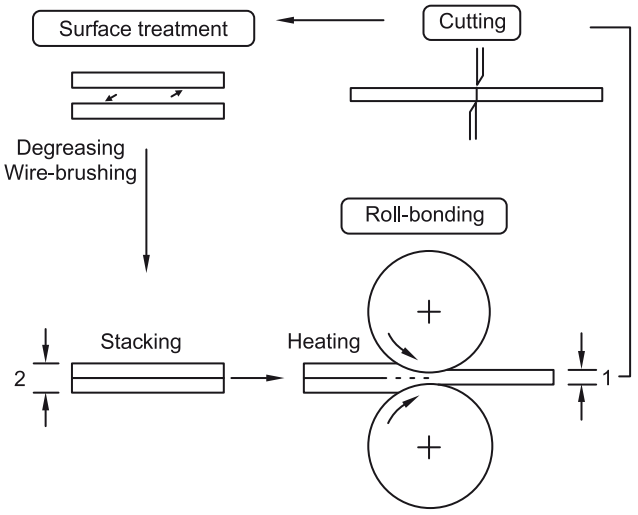

Fig. 3.22 Principle of accumulative roll bonding.

rolling force is large in comparison with conventional rolling. Except for the necessity of large enough capacity of the rolling mill which can realise one-pass heavy roll bonding, there are no special requirement in the equipments for the ARB. A serious problem in the ARB process is fracture of the materials. Since a large amount of total plastic strain is accumulated in the materials, the rolling is not a hydrostatic process; edge-cracks sometimes appear in the sheets, especially at higher cycles. In certain kinds of materials, such as Al–Mg alloy, the edge cracks largely propagate into the centre of the sheets. In that case, it becomes impossible to proceed to the subsequent cycles. With ductile materials, for example, pure aluminum and iron, the UFG sheets with dimension $1 \times 50 \times 300$ mm are fabricated without cracking by the ARB process.

Irrespective of the kind of material studied, the average grain diameter of UFG materials is around 500 nm. The UFGs are surrounded by clear but irregular-shaped boundaries; the number of dislocations inside the grains seems small. These features are similar to those observed in materials that have been heavily deformed by other SPD processes. The most characteristic feature of the UFGs in the ARB-processed materials is the elongated morphology. Measurements clearly confirm that the elongated UFGs are not subgrains, but are grains surrounded by high-angle grain boundaries.

ARB-processed materials with elongated UFG structures exhibit very high strength. The grain size and the tensile strength of the various UFG materials fabricated by ARB are summarised in Table 3.5. In most cases, the mean grain thickness of the pancake-shaped UFGs or the ultrafine lamellar structures are 100 ~ 200 nm. Materials with higher purity tend to show larger grain size. ARB at lower temperature results in smaller grain size within the similar materials. UFG materials exhibit tensile strength which is two to four times higher than that of the starting materials with conventional grain sizes. On the other hand, ARB-processed materials have limited tensile elongation owing to early plastic instability.

Table 3.5 Grain size and tensile strength of various ARB-processed metals and alloys

Materials (wt.%)	ARB process	Grain size (nm)	Tensile strength (MPa)
4N-Al	7 cycles RT	670	125
100-Al (99%Al)	8 cycles RT	210	310
5052-Al (Al–2.4Mg)	4 cycles RT	260	388
5083-Al (Al–4.5Mg-0.6Mn)	7 cycles at 100°C	80	530
6061-Al (Al–1.1Mg–0.6Si)	8 cycles RT	100	357
7075– l (Al–5.6Zn–2.6Mg–1.7Cu)	5 cycles at 250°C	300	376
OFHC-Cu	6 cycles RT	260	520
Cu–0.27Co–0.09P	8 cycles at 200°C	150	470
Ni	5 cycles RT	140	885
IF steel	7 cycles at 500°C	210	870
0.041P-IF	5 cycles at 400°C	180	820
SS400 steel (Fe–0.13C–0.37Mn)	5 cycles RT	110	1030
Fe–36 Ni	7 cycles at 500°C	87	780

3.2.5 Nanolithography

STM-based nanolithography This has been exploited for local oxidation and passivation, localized chemical vapour deposition, electrodeposition, mechanical contact of the tip with the surface, and deformation of the surface by electrical pulses. Patterns with a minimal size from 10–20 nm to 1 nm in ultrahigh vacuum (UHV) have been demonstrated. Nanometre-sized holes can be formed using low energy electrons from a scanning tunnelling microscope (STM) tip when a pulsed electric voltage is applied in the presence of sufficient gas molecules between the substrate and the tip. For example, holes that are 7 nm deep and 6 nm wide on highly ordered pyrolytic graphite (HOPG) substrate were formed in nitrogen at a pressure of 25 bar by applying a 7 V pulse to the tip for 130 mins, with the distance between the tip and the substrate being 0.6–1 nm. A possible mechanism is that the electric field induces the ionisation of gas molecules near the STM tip, and accelerates the ions towards the substrate. Ions bombard the substrate and, consequently, nanometre-sized holes are created. A certain electric field is required to generate field emitted electrons. The diameter of an electron beam ejected from an STM tip is dependent on the applied bias voltage and the diameter of the tip. At low bias (<12 V), the diameter of the ejected electron beam remains almost constant; however, the beam diameter changes significantly with bias voltage and the diameter of the tip.

Nanostructures can be created using field evaporation by applying bias pulses to the STM tip–sample tunnelling junction. For example, nanodots, nanolines, and nanocorrals of gold on a clean stepped Si (111) surface were fabricated by applying a series of bias pulses (< 10 V and ~30 μs) to an STM gold tip at UHV (a base pressure of 10^{-10} mbar). Nanodots with diameter as small as a few nanometres can be realised. By decreasing the distance between adjacent nanodots, it was possible to create continuous nanolines, a few nanometres wide and over a few hundred nanometres long. A nanocoral of diameter about 40 nm, formed by many Au nanodots, each with diameter of a few nanometres, was also created on the Si (111) surface.

AFM-based nanolithography Direct contacting, writing or scratching is referred to as a mechanical action of the AFM tip that is used as a sharply pointed tool in order to produce fine grooves on sample surfaces. Although direct scratching creates grooves with high precision, low quality results are often obtained due to tip wear during the process. An alternative approach is to combine scratching on a soft resist polymer layer, such as PMMA or polycarbonate, as a mask for the etching process and subsequent etching to transfer the pattern to the sample surface. This method ensures reduced tip damage, but also precludes an accurate alignment to the structures underneath. A two-layer mask has been investigated as a further improvement. For example, a mask coating consisting of a thin layer of polycarbonate of 50–100 m and a film of an easy-to-deform and fusible metal such as indium or tin was used to create 50 nm–wide structures. Figure 3.23 is a typical layout of the sample and process steps with AFM lithography.

Dip-pen nanolithography In dip-pen nanolithography (DPN), the tip of an AFM operated in air is 'inked' with a chemical of interest and brought into contact with a surface. The ink molecules flow from the tip onto the surface similar to a fountain pen. The water meniscus that naturally forms between the tip and the surface enables the diffusion and transport of the molecules, as shown in Fig. 3.24. Inking can be done by dipping the tip in a solution containing a small concentration of the molecules, followed by a drying step (e.g., blowing dry with compressed difluoroethane). Line widths down to 12 nm with spatial resolution of 5 nm have been demonstrated with this technique. Species patterned with DPN include conducting polymers, gold, dendrimers, DNA, organic dyes, antibodies and alkanethiols. Alkanethiols have also been used as an organic monolayer mask to etch a gold layer, and subsequently etch the exposed silicon substrate.

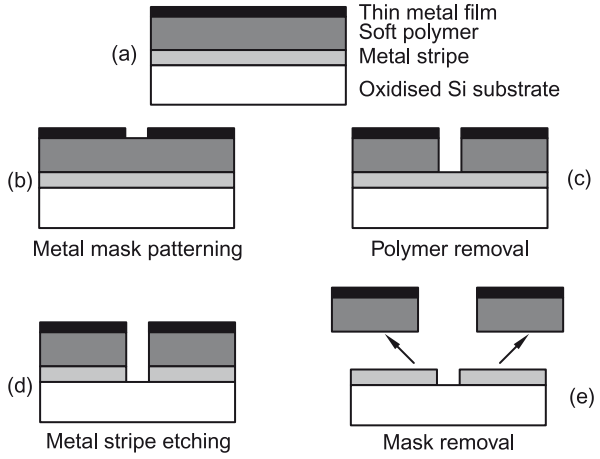

Fig. 3.23 Layout of the sample and the process steps with AFM lithography: (a) sample multilayer structure, (b) thin mask patterning by AFM lithography, (c) polymer removal in plasma oxygen, (d) titanium stripe etching, and (e) resulting electrodes after sacrificial layers removal.

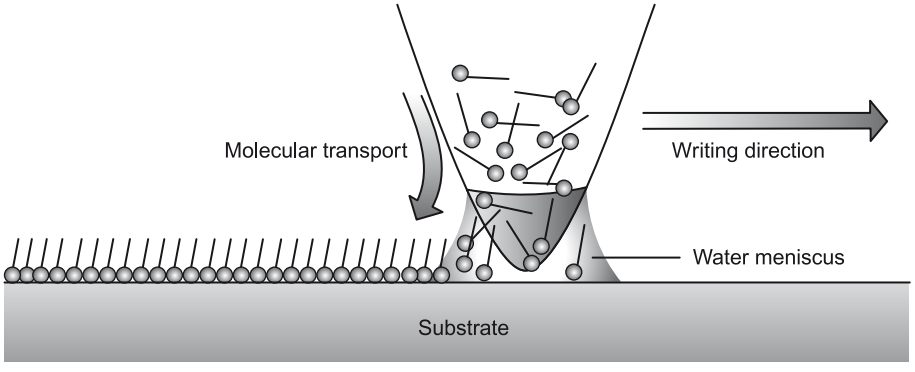

Fig. 3.24 Schematic representation of the working principle of dip-pen nanolithography.

3.3 CONSOLIDATION OF NANOPOWDERS

The commercial application of nanomaterials beyond the boundaries of materials science laboratories is possible only on successful consolidation of these materials into bulk-sized components preserving the nanostructures. Due to the long duration of sintering at high temperature that is involved in conventional consolidation techniques, it is difficult to retain the nanograin-size due to grain growth in such techniques.

The density of the green compact depends on the frictional forces of the powder particles that originate from electrostatic, van der Waals and surface adsorption forces. These forces are significantly high in nanoparticles, forming hard agglomerates and inter-agglomerates, which are relatively large. Further, nanoparticles contain a large number of pores which require not only higher temperature but also prolonged sintering times for their successful elimination; consequently, it becomes difficult to retain the grain size in the nanometre domain. Large pores undergo pore–boundary separation that restricts the attainment of full density in the consolidated nanoparticles. During sintering of nanoparticles, pores smaller than the critical size shrink, while larger pores undergo pore–boundary separation. The fraction of grain boundaries in nanomaterials is large compared to that in coarse-grained materials. The density of the grain boundary regions is less than the grain interior due mainly to the relaxation of atoms in the grain boundaries; they also contain other lattice defects. Therefore, consolidated nanoparticles with retained nanostructure are expected to exhibit a density lower than the theoretical density of the bulk counterpart.

There are numerous conflicting views on the sintering behaviour of nanoparticles. Nanoparticles show depressed onset of sintering temperature to the range of 0.2 T_m–0.3 T_m compared to conventional powders that normally exhibit a range of 0.5 T_m–0.8 T_m, where T_m is the melting point (in K). Cu–Ta nanocomposites have been consolidated to close to theoretical densities at 500°C, while the microcomposites in the same system need a sintering temperature of 1000°C (Fig. 3.15). Similarly, W, which is used in filaments, is usually sintered at about 2800°C due to its high melting point. However, nanocrystalline W could be sintered to close to its theoretical density at 1500°C itself leading to significant energy savings. Figure. 3.25 shows the dilatometry results of microcrystalline W and nanocrystalline W (50 mm) obtained by high-energy ball milling of W (50 mm) in Simoloyer for two hours. Significant differences in sinterability are evident from the extent of consolidation observed in the nanocrystalline W. Such results may possibly be attributed to significantly high diffusivities due to large surface/grain boundary area and large defect densities.

Synthesis of nanoparticles of ceramic, metallic and their mixture has made substantial progress in the last decade. However, retention of nanostructures in these materials after consolidation into fully dense components is a challenge. A brief review of the various consolidation processes is presented here.

3.3.1 Shockwave consolidation

Shock wave consolidation, also termed *dynamic consolidation*, is used to densify powdered materials without inducing thermal activated microstructural and compositional changes

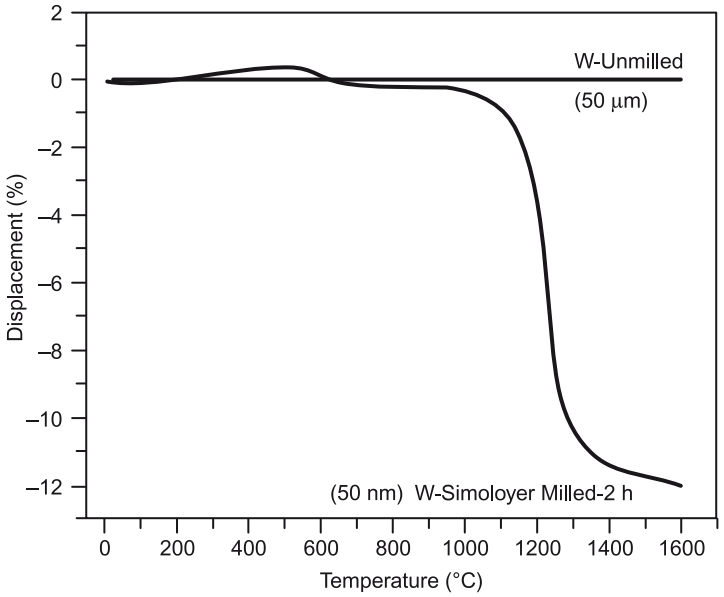

Fig. 3.25 Improved sinterability of nanocrystalline W in comparison to microcrystalline W. (*Source:* BS Murty, IIT Madras).

that are normal in conventional thermomechanical processing. Such densification is possible because of the interparticle bonding due to localized melting at the interfaces between the particles. High pressure and rapid loading rates that create high plastic deformation finally lead to high shock initiated chemical reactions completely different from the conventional ones. Metallic or alloy powders are usually processed through this route due to the fact that plastic deformation in metal is comparatively easier than for ceramics.

In this process, particles are enclosed in a steel block that looks similar to a cold compaction chamber that is covered using a plate, on top of which a driver plate usually bears the brunt of explosions and drives the shock wave towards the sample (Fig. 3.26). The driver plate is usually made of highly conductive and ductile material. Explosives are packed on top of this plate carefully and the spillage, if any, has to be removed. The detonator is set on top of the explosive and the set up is ready for processing to start. Ammonium nitrate is usually used as the explosive. Shock compaction of powders is a dynamic consolidation technique which provides a viable method for densification of amorphous as well as ultrafine powders. Fe-, Ni- and Ti-based alloys have been studied more often using this technique. Pure metals and alloys with retained nanostructures can be consolidated using this technique. Some of the systems that have been investigated are: $Fe_{73.5}Cu_1Nb_3Si_{13.5}B_9$, Fe, Fe–Al, diamond–Si, Al, $Pr_2Fe_{14}B/\alpha$-Fe, Ti_5Si_3 and NiAl.

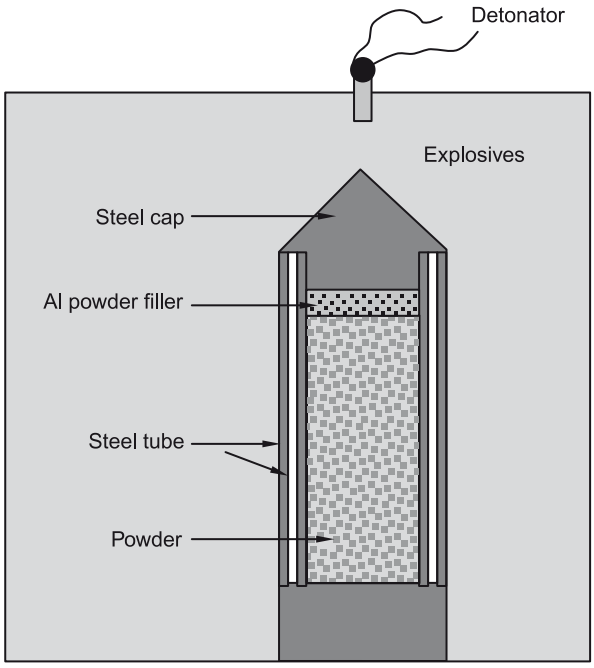

Fig. 3.26 Schematic of shock wave consolidation setup.

3.3.2 Hot isostatic pressing (HIP) and cold isostatic pressing (CIP)

The process of using high hydrostatic pressure and high temperature to compress fine particles into coherent parts is termed 'hot isostatic pressing' (HIPing). This process provides a method for producing components from diverse powdered materials, including metals and ceramics. A typical schematic of the HIPing process is shown in Fig. 3.27. In this process, the elemental blend is placed in a container, usually a steel can. The container is subjected to elevated temperatures, and very high vacuum to remove air and moisture from the powder, after which it is sealed and HIPed. The application of high inert gas pressures and elevated temperatures results in the removal of internal voids and creates a strong bond throughout the material. The result is a clean homogeneous material with a uniformly fine grain size and near 100% density.

In cold isostatic pressing (CIPing), pressure is applied from multiple directions to get better uniformity of compaction, compared to uniaxial pressing. There are two methods in isostatic pressing. In wet bag isostatic pressing, the powder is encased in a rubber sheath that is immersed in a liquid that transmits the pressure uniformly to the powder. In dry bag isostatic pressing, instead of immersing the tooling in a fluid, the tooling itself is built with internal channels into which high pressure fluid is pumped.

Some of the material systems that have experimented with the HIPing process are TiC, TiCN, SiC, Si_3N_4–Y_2O_3–Al_2O_3, Si_3N_4, intermetallic TiAl, TiAlSi, $MgAl_2O_4$, Ni–Fe, Y_2O_3 dispersed steels, $MgAl_2O_4$ dispersed steels, Al and carbon nanotube reinforced Si_3N_4. There have been instances where HIP is used as an add-on processing to CIP to increase the densification and thereby mechanical properties, for example, consolidation of Fe. Using CIP as a primary consolidation technique works well for a micron-sized particle whereas a nanoparticle might need some kind of secondary consolidation process to form a bulk part, as the nanoparticles are friable and can crumble even if crushed with a hand. The only solution is to either use sintering after CIPing or to use HIPing. It has been found that HIPing leads to better densification in less time compared to the time required for sintering to achieve the same density.

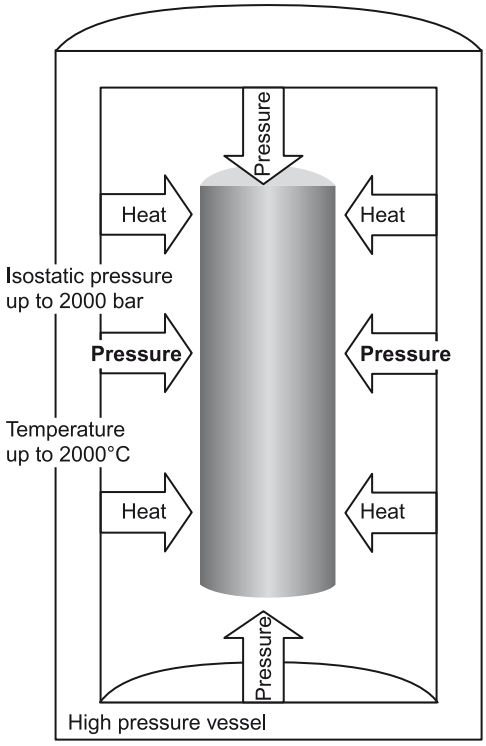

Fig. 3.27 Schematic of a hot isostatic pressing setup.

3.3.3 Spark plasma sintering

With the growing need for processing and consolidating nanopowders, retaining the initial microstructure in the fabricated component remains a challenge. Though the manufacture of novel materials is limited to laboratory scale, vigorous demand in the market persists and is driving the demand for new consolidation techniques apart from hot pressing, high temperature extrusion and hot isostatic pressing. Since longer processing times at high temperatures often result in extraneous grain growth, the new nanopowder processing technique, namely spark plasma sintering (SPS), which has evolved in the last decade, overcomes these obstacles by applying rapid heating to sintering temperatures, leading to rapid sintering of nanocomposites. The attractive properties of nanopowders are well conserved by the fabrication of bulk material through SPS. Consolidation of metals, composites, ceramics, intermetallics, cermets, nanocomposites and carbon nanotube reinforced ceramics has been accomplished by spark plasma sintering.

The schematic of a typical SPS apparatus is shown in Fig. 3.28. It consists of a graphite die where powder is loaded and heated by passing an electric current. Hold time, ramp rate, pulse duration, and pulse current and voltage can be set for controlling the temperature of the sintering cycle. Change in temperature, pulse power (voltage/current), sintering displacement

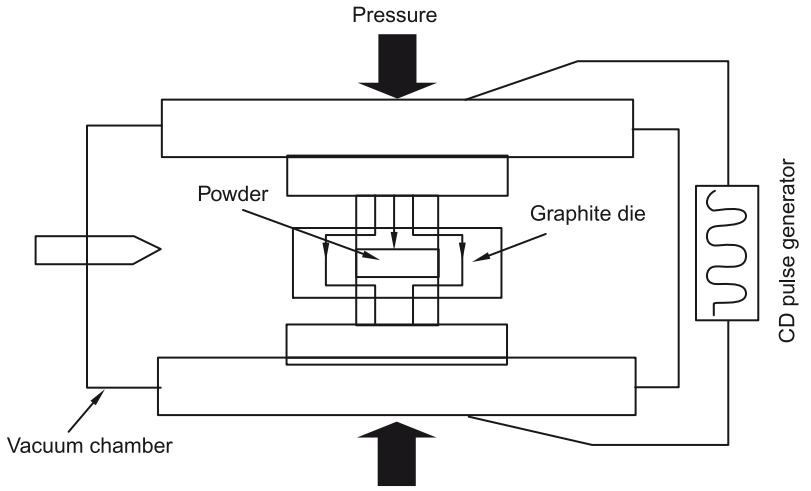

Fig. 3.28 Schematic of SPS setup.

and sintering rate are recorded in situ during spark plasma sintering. Powder mixtures are initially cold pressed (~ 200 MPa) into a compact disc (with diameter around 2 cm and thickness around 5 mm), followed by SPS processing to produce nano-consolidated nanocrystalline composites. Typical SPS processing parameters include:

- Applied pressure between 50 and 100MPa
- Pulse duration of ~ 10 ms with on–off cycle of 2–2.5 ms
- Maximum pulse parameter of 10,000 A and 10 V

After applying the given pressure, samples are heated to the preset temperature (for a few minutes) and are ramped rapidly (~150–500 K/min) to sintering temperatures with hold time of 3–5 min to complete the sintering. Samples are usually cooled to below 100°C within 5 minutes of the completion of sintering.

Densification of the green compact occurs in four stages: vacuum creation, pressure application, resistance heating and cooling down as shown schematically in Fig. 3.29. SPS is carried out in vacuum to account for removal of gases, and results in a densely consolidated composite. Heating is accomplished by spark discharge between particles, which activates the surface by removing surface oxide. This helps in heat and mass transfer between the purified particles to carry heat and sinter them to full density. Initially, samples show an increase in volume due to thermal expansion, followed by shrinkage occurring primarily during resistance heating when the green discs are held at high temperatures and pressure. Onset of sintering is dependent on the initial particle size, which decides the onset of shrinkage. It is generally difficult to determine when the sintering process is complete; however, shrinkage of the specimen could help in deducing the completion of SPS sintering. Some of the nanopowder material systems that have been consolidated with SPS process are amorphous Si–C–N, Ni–Ti shape memory alloy, $(Al–12.5Cu)_3Zr$ intermetallic, TiCN cermet, $SiC–ZrO_2–Y_2O_3–Al_2O_3$

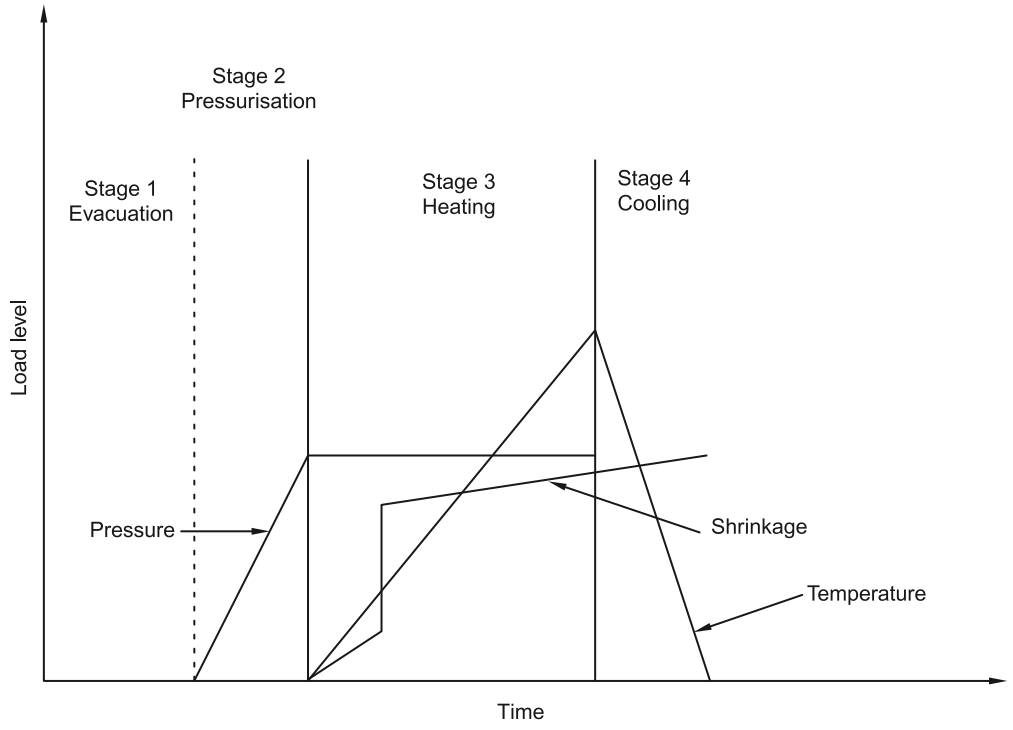

Fig. 3.29 Schematic of SPS sintering stages.

composites and CNT-Al_2O_3 composites. Figure 3.30 shows the TEM images of SPS consolidated structural nanocomposites (NiAl–Al_2O_3 and FeAl–Al_2O_3), both of which demonstrate that the nanocrystalline nature is retained after SPS.

Considering the rapid advancement in the field, it is a mammoth task to cover all the techniques of synthesis and consolidation of nanoparticles and nanocrystalline materials that are available, and the reader is encouraged to further explore this exciting world.

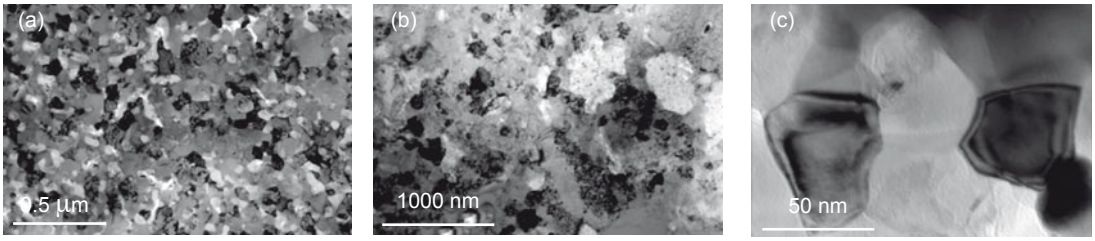

Fig. 3.30 TEM images of SPS consolidated samples of (a) NiAl–Al_2O_3 and (b) FeAl–Al_2O_3 nanocomposites; (c) Higher magnification image of a region in (b). (*Source:* BS Murty, IIT Madras).

SUMMARY

- Various techniques are available for the synthesis of nanoparticles and nanostructured materials.
- The techniques available can be grouped broadly into the 'top-down' and 'bottom-up' approaches.
- These techniques can also be classified, based on the state of the matter from which the nanomaterials are synthesized.
- In bottom-up techniques, nanoparticles are prepared from the vapour or liquid phase, while in top-down approaches, they are made from solids.
- The challenge in consolidation of nanoparticles is to retain the nanocrystallinity after consolidation.
- Among the various techniques of consolidation, spark plasma sintering is popular.

EXERCISES

1. Define 'top-down' and 'bottom-up' approaches for the synthesis of nanomaterials.
2. Identify the category (top-down or bottom-up) to which the methods listed below belong:
   (a) Sol–gel
   (b) MBE
   (c) E-Beam lithography
   (d) ECAP
   (e) Wire explosion
   (f) Laser ablation
3. Describe the principle involved with suitable figures in the following techniques:
   (a) RF and DC sputtering
   (b) Electron beam evaporation
   (c) Microwave plasma based CVD
4. It is desired to synthesize yttria nanoparticles of about 2–3 nm in size. Discuss the suitability of the following techniques for the purpose with reasoning.
   (a) Mechanical milling, (b) Electron beam evaporation, (c) CVD, (d) Sol–gel
5. Identify a suitable technique for the synthesis of (a) Au nanoshells and (b) Silica nanoshells, and list a few applications for each.
6. Describe the distinctive features of a self-assembled nanostructure.
7. Compare ion and electron beam nanolithography for nanofabrication.
8. List a few deformation-based techniques for the development of nanostructures.
9. Discuss briefly what we can learn from nature for the synthesis of nanostructures.
10. Identify techniques for the development of bulk nanostructured solids from nanopowders.